SEISMIC EXPRESSION, STRUCTURE AND EVOLUTION OF FLOW CELLS WITHIN A MASS-TRANSPORT COMPLEX

HARYA D. NUGRAHA[1,2†*], CHRISTOPHER A-L. JACKSON[1,3†], HOWARD D. JOHNSON[1], and DAVID M. HODGSON[3]

[1]Basins Research Group (BRG), Imperial College, London SW7 2BP, UK
[2 †]Center for Sustainable Geoscience, Universitas Pertamina, Jakarta 12220, Indonesia
[3 †]Department of Earth and Environmental Sciences, The University of Manchester, Manchester M13 9PL, UK
[4]Stratigraphy Group, University of Leeds, Leeds LS2 9JT, UK
**email: harya.nugraha14@imperial.ac.uk*
[†:]Present address

Keywords: submarine landslide, mass-transport complex, seismic reflection, intra-flow shear, flow cells

ABSTRACT

Mass flows evolve longitudinally during emplacement, but they can also vary laterally by forming discrete, shear zone-bound intraflow cells with different rheological states. Despite being documented in several field and subsurface studies, the controls on the initiation, translation, and cessation of these flow cells remain unclear. We here use five, high-quality post-stack time-migrated (PSTM) 3D seismic reflection datasets to define the seismic expression and investigate the structure and evolution of flow cells in the Gorgon Slide, a near-seabed mass transport complex (MTC) on the Exmouth Plateau, offshore NW Australia. The slide originated from a 30 km-wide, NE-trending headwall scarp that dips steeply (*c.*30°) seaward and travelled northwestwards over a basal-shear surface that deepens downslope. The slide is dominated by chaotic seismic reflections, which are interpreted as debrite, containing seismically-imaged megaclasts (*c.*0.05-1 km-long) derived from the slide's headwall. The morphology and orientation of the basal-shear surface focused slide transport, resulting in the clustering of megaclasts in proximal parts of the translation domain. The megaclast cluster became an obstacle to flow, which resulted in the formation of two flow cells (Cells A and B), separated by a longitudinal shear zone. The interaction between the two cells is recorded by the development of sinuous flow fabrics within, and pressure ridges on the top surface of, the slide. Along

the longitudinal shear zone, the flow fabrics and ridges in Cell A were dragged downslope by the relatively faster and/or longer-lasting Cell B, which continued translating downslope in the absence of any intraflow obstacles. The transport processes of the Gorgon Slide show how entrainment and abrasion of megaclasts induced velocity perturbations during emplacement causing: (i) changes to the flow rheology, and (ii) the initiation and cessation of flow cells. A better understanding of how flow cells evolve during MTCs transport may help to refine modelling of the potential impact of MTCs on submarine infrastructure.

INTRODUCTION

The degradation of submarine slopes drives emplacement of large mass-transport complexes (MTCs), which result from gravity-driven depositional processes that include slides, slumps and debris flows (e.g. Dott 1963; Nardin et al. 1979; Nemec 1991; Moscardelli and Wood 2008; Posamentier and Martinsen 2011). Slope degradation and MTC emplacement not only influence continental margin evolution (e.g. Gamboa et al. 2010) and petroleum system development (e.g. Weimer and Shipp 2004), but they also pose a significant geohazard for coastal and offshore infrastructure (e.g. Parker et al. 2008; Randolph and White 2012; Vanneste et al. 2013). Potentially mitigating the effects of MTC-related geohazards is essential and partly depends on a good understanding of MTC emplacement processes (Masson et al. 2006). For example, the rheology and emplacement direction of an MTC can evolve during transport (Iverson 1997; Dykstra et al. 2011; Joanne et al. 2013; Ortiz-Karpf et al. 2017; Hodgson et al. 2018), which may influence the amount and direction of drag forces exerted on submarine pipelines (e.g. Zakeri 2009).

Transport processes within MTCs are dynamic. A large, single (first-order) flow cell (i.e. a kinematically linked, downslope-travelling sediment mass) can evolve as it translates due to: (i) the ingestion of ambient water, which serves to dilute the flow and potentially increase intraflow turbulence (Fisher 1983; Talling et al. 2012; Sun et al. 2018); and/or (ii) the formation of smaller, second-order (intra-

MTC) flow cells due to internal velocity variations (Alsop and Marco 2014). In contrast to the processes driving rheological transformations between turbidity current and debris flow processes, the origin of flow cells remain poorly documented. Although the structure, kinematics and origin of flow cells have been inferred from relatively small-scale outcrop studies of individual slump sheets (Farrell 1984; Alsop and Marco 2014), limited outcrop extent invariably hampers a full three-dimensional analysis. Studies using 3D seismic reflection data have also documented the presence of intra-MTC flow cells at significantly larger scales (Gee et al. 2005; Bull et al. 2009; Steventon et al. 2019). However, the mechanisms responsible for the initiation, translation, and cessation of these flow cells, across a range of scales, remain poorly understood. This work demonstrates that individual cells move at the same time but at different speeds within a translating mass, and/or may even translate at different times, as indicated by flow fabrics and longitudinal shears within and on the top surface of their host MTCs (*sensu* Bull et al. 2009).

Here, we use five high-quality 3D seismic reflection datasets from the Exmouth Plateau (offshore NW Australia) to study a recent MTC, the Gorgon Slide (hereafter the 'slide') that is interpreted to contain two large-scale flow cells (Fig. 1). The 3D seismic reflection datasets image most of the Gorgon Slide enabling us to characterise the full extent of the slide (Fig. 1C). As the slide is at, or just below, the seabed, detailed seismic attribute analysis allows us to: (i) document kinematic indicators on basal-shear and top surfaces, and within internal body of the slide; (ii) use these kinematic indicators to reconstruct the slide emplacement processes and to delineate flow cells; (iii) infer the impact of flow cell formation and evolution on overall flow behaviour; and (iv) consider potential factors controlling the formation of the flow cells.

DATA AND METHODOLOGY

The five, high-quality post-stack time-migrated (PSTM) 3D seismic reflection datasets image *c.*93% (i.e. 1594 km^2 of 1760 km^2 total area) of the Gorgon Slide, covering all of the evacuation zone and most of the deposition zone (Figs. 1B-C). We used three 2D seismic reflection lines to constrain the downdip limit of the deposition zone (green lines in Fig. 1C). The vertical resolution of the 3D seismic reflection data at the base of the slide (*c.*500 m below sea floor) ranges from 8-11 m, based on near seabed sediment velocity and dominant seismic frequency of 1824 m/s and 40-60 Hz, respectively. Bin spacing of the 3D seismic volumes ranges from 12.5 x 18.75 m to 20 x 25 m (see Appendix 1 for details). Depth conversion of seabed and basal-shear surface time-structure maps was conducted by using average seismic velocities for water (1519 m/s) and weakly compacted, near-seabed sediment (1824 m/s), respectively (Appendix 1). The average water velocity is constrained by ten industry wells (Fig. 1B), and the near-seabed sediment velocity data is available from well ODP 762 (see Figs. 1A and 2).

We mapped the seabed and basal-shear surface of the Gorgon Slide to define its kinematics as it initiated, translated, and arrested. We also employed an iso-proportional slicing method (Zeng et al. 1998), midway between the seabed and basal-shear surface of the slide, to visualise and map the heterogeneity of its constituent seismic facies. Several seismic attributes were used in this analysis, particularly: (i) *variance*, to better image discontinuities (Chopra and Marfurt 2007), including grooves on the basal-shear surface of an MTC (e.g. Bull et al. 2009); (ii) *Root Mean Squared (RMS) Amplitude*, to better delineate features that have distinct positive or negative amplitudes resulting from an acoustic (velocity and/or density) contrast (Brown 2011), such as megaclasts encased within a relatively transparent debritic matrix (e.g. Ortiz-Karpf et al. 2017); (iii) *dip*, to better image rugosity of a surface (Brown 2011), including seabed relief (e.g. Bull et al. 2009); and (iv) *spectral decomposition*, to highlight internal stratigraphic (seismic facies) heterogeneities within a geological body such as a mass-transport complex (Partyka et al. 1999; Eckersley et al. 2018).

GEOLOGICAL SETTING

The Exmouth Plateau is a part of North Carnarvon Basin (NCB), which has experienced multiple rifting events from the Late Jurassic to Early Cretaceous (Fig. 2) (Tindale et al. 1998; Longley et al. 2002).

Post-rift deposition was initially dominated by fine-grained siliciclastic sediments, becoming carbonate-dominated as the Australian plate drifted northward towards the equator (e.g. Apthorpe 1988; Hull and Griffiths 2002). Clinoforms demonstrate progradation of the carbonate-dominated margin from the Oligocene to the present-day (Fig. 2B) (Cathro et al. 2003; Moss et al. 2004). Collision between the Australian and Eurasian plates (Miocene to present-day) has reactivated some of the rift-related faults, forming inversion structures such as the NE-trending Exmouth Plateau Arch (Fig. 2) (Keep et al. 1998). It is likely that inversion-related deformation of the seabed triggered the widespread emplacement of the numerous MTCs across the plateau (Boyd et al. 1993; Hengesh et al. 2013; Scarselli et al. 2013). Presently, pelagic carbonate sediments dominate the depositional style, with sedimentation rates being as low as 20 m/Myr (Golovchenko et al. 1992). We focus on the Gorgon Slide, which extends from the seabed (blue) down to its basal-shear surface (yellow, see Fig. 2B). The headwall of the Gorgon Slide is underlain by a rift-related horst block, which was drilled by Bluebell-1 (Fig. 2B) (McCormack and McClay 2013). This horst contains the giant Gorgon gas field, containing 11 tcf of gas in place (Clegg et al. 1992).

THE GORGON SLIDE

General Characteristics

External geometry and morphological domains.--- The Gorgon Slide was sourced from the slope defining the present-day shelf-edge of NW Australia (Fig. 1). It was deposited in the adjacent Kangaroo Syncline, forming a lenticular, NW-trending body that wedges-out (i) to the SE against the continental slope, and (ii) to the NW against the eastern margin of the Exmouth Plateau Arch (see Figs. 1B-C and 2). The slide has a maximum runout distance of *c.*70 km, is up to 500 m-thick, and has a total volume of *c.*500 km^3 (Fig. 3A) (Nugraha et al. 2019a). The slide terminates against two lateral margins (to the NE and SW), being *c.*30 km-wide in the central part and abruptly narrowing to *c.*18 km at its frontal end (Fig. 3A). Downdip changes in the slide width results in two frontal margins (eastern and western), separated by *c.*10 km in the dip-direction by a NW-trending lateral margin (Fig. 3A).

The central and frontal parts of the slide display a notable along-strike change in seabed rugosity, which defines two distinctive regions: Areas A and B (Fig 3B). Area A is bound by the NE lateral and eastern frontal margins and is characterized by a highly rugose seabed (Fig. 3B). In Area B, which is bound by the SW lateral and western frontal margins, the seabed is relatively smoother than that of Area A (Fig. 3B). Areas A and B are separated by a linear, NW-trending feature (see zoomed-in image in Fig. 3B) that is subparallel to both lateral margins of the slide. This feature is narrow (*c.*170-300 m-wide) and extends for *c.*26 km updip, apparently dying-out where Areas A and B are indistinguishable, and merging downdip with the NE lateral margin of Area B near the slide terminus (see Figs. 3B-C). This feature marks a change in seabed relief of *c.*10-20 m between Areas A and B (Fig. 3C).

The Gorgon Slide originated from a *c.*18 km-long evacuation zone, bound on its updip margin by a steeply-dipping (*c.*30°), *c.*350 m-high headwall scarp (Fig. 4A). The frontal margin of Area A is clearly marked by positive seabed relief (*c.*30 m) relative to the smooth seabed bounding pre-slide slope strata immediately downdip. Pre-slide strata are represented by older MTCs (i.e. chaotic, weakly reflective seismic reflections), and hemipelagic and pelagic slope strata (i.e. continuous, reflective, sub-parallel seismic reflections) (Fig. 4A). The depositional variability of pre-slide strata and across-strike changes defines different slide termination styles (Fig. 4B): (i) the SW lateral margin defines the pinch-out of the slide onto hemipelagic or pelagic slope strata on the NE flank of the Exmouth Plateau Arch, and (ii) the NE lateral margin marks a strongly erosional boundary with an older MTC and underlying non-MTC slope strata. Inferred hemipelagic and pelagic slope strata capping the older MTC are cross-cut and overlain by a thin fringe of the younger Gorgon Slide.

The linear zone on the seabed (Figs. 3B-C) is interpreted as a longitudinal shear zone (*sensu* Bull et al. 2009), which records internal variations of transport velocity within an MTC. Locally, the longitudinal shear zone not only defines the change of seabed relief between Areas A and B, it could also coincide with positive seabed relief (Fig. 4B). This longitudinal shear zone is interpreted here because it later helps us define and describe different structural domains within the slide.

Internal seismic facies.– The internal character of the Gorgon Slide is variable, and a seismic facies classification captures this internal heterogeneity (Fig. 5). This classification also illustrates variations in the degree of internal stratal disaggregation, which we relate to sediment transport processes (e.g. Alves et al. 2014). Our classification builds on previous studies that have calibrated seismic reflection data with lithology from well data (e.g. Sawyer et al. 2009), and seismic reflection forward model constructed using field data (Dykstra et al. 2011). Five seismic facies (SF) are defined in this study (Fig. 5A) based on variability in internal reflection configurations in cross-section and plan-view (see Figs. 5B-G): (i) SF-1 - mostly transparent with low-to-variable amplitude reflections, which are interpreted as debrites (cf. Posamentier and Kolla 2003; Posamentier and Martinsen 2011; Ortiz-Karpf et al. 2017); (ii) SF-2 - low-to-medium amplitude, discontinuous, folded reflections in cross-section that occasionally define sinuous lineations in plan-view, which are also interpreted as debrites containing partially disaggregated material; (iii) SF-3 - contains high-amplitude, folded reflections that are offset by thrusts, interpreted as fold and thrust systems; (iv) SF-4 - isolated packages of coherent, sub-parallel, variably deformed features surrounded by SF-1 and -2, interpreted as megaclasts embedded within the debritic matrix (cf. McGilvery 2004; Bull et al. 2009; Jackson 2011; Ortiz-Karpf et al. 2017; Hodgson et al. 2018); and (v) SF-5 - sub-parallel and continuous reflections that characterise non-MTC, predominantly pre-slide slope strata (see Fig. 4A) (e.g. Prélat et al. 2015). The *c.*26 km-long, NW-trending linear feature described above is generally characterised by SF-1 (Fig. 3C) (i.e. debrite) (cf. Ogata et al. 2014; Bull and Cartwright 2019; Omeru and Cartwright 2019), although its relatively narrow width means it can be difficult to differentiated it from adjacent deposits within Area A and B where more continuous reflections (i.e. megaclasts) are not juxtaposed (Figs. 4B, and 5B-E).

Having provided a general overview of the external geometry, scale, and inferred composition of the Gorgon Slide, we now provide a systematic description of its primary kinematic indicators and interpret the related emplacement processes from its four principal domains: (i) headwall domain; (ii) upper translation domain (UTD); (iii) lower translation domain (LTD); and (iv) toe domain (Fig. 3B).

Headwall domain

Description.– The largest feature in the headwall domain is a large, NW-dipping scarp (see above) (Fig. 6). Immediately updip of this feature are: (i) a small, NNE-trending scarp, next to which are (ii) numerous circular depressions that have diameters of *c.*100-300 m, and (iii) at least four, *c.*3-5 km-long, *c.*15 m-deep, linear depressions (see zoomed-in image in Fig. 6A). Downdip of the headwall scarp, within the source area of the Gorgon Slide (i.e. the region between the headwall scarp and evacuation-deposition zone boundary), there are numerous *c.*5-16 km-long, broadly NW-SE trending, elongate features (Figs. 6A-B) that have a v-shaped geometry in cross-section, which are (*c.*150-300 m-wide and *c.*10-25 m-deep (see zoomed-in image in Fig. 6B).

Interpretation.– The small scarp (*c.*10 m-high) is cross-cut by, and thus older than, the main headwall scarp (Fig. 6B). The circular depressions are interpreted as pockmarks (e.g. Hengesh et al. 2013; Scarselli et al. 2013), which could indicate active vertical fluid expulsion. The linear depressions are interpreted as crown cracks, possibly marking the location of future slope failure events (Varnes 1978; Frey-Martinez et al. 2005). We interpret the elongate features with v-shaped cross-sectional geometry as grooves (*sensu* Bull et al. 2009) formed due to tooling by megaclasts into the substrate during slide transport (Posamentier and Martinsen 2011; Ortiz-Karpf et al. 2017; Hodgson et al. 2018; Sobiesiak et al. 2018). Based on their orthogonal relationship with the headwall scarp, these grooves are a reliable indicator of the translation pathway of the slide through the evacuation zone.

Evacuated volume.–The initial failed volume of the Gorgon Slide that was removed from the headwall domain ranges from 31 to 43 km^3, which is 12-16 times smaller than the deposited volume (*c.*500 km^3) (Nugraha et al. 2019a). This volume discrepancy is interpreted as a result of significant erosion and substrate entrainment of the carbonate ooze substrate during transport (see Nugraha et al. 2019a).

Upper translation domain

Description.– Grooves in the updip part of the upper translation domain (Fig. 7A) are the downdip continuation of those within the evacuation zone (see Fig. 6), displaying similar dimensions and geometries (see Headwall domain section). However, grooves in this domain converge downslope towards the NE lateral margin (Fig. 7A), which contrasts to the more commonly described downslope-diverging grooves (e.g. Posamentier and Kolla 2003; McGilvery 2004; Ortiz-Karpf et al. 2017). In the central part of the basal-shear surface is a pair of broadly NW-trending, slightly curved lineations that bound an area slightly elevated (*c.*10 m) compared to its surrounding area, and which mark subtle changes in the depth of the basal-shear surface (medium grey-shaded grey in Fig. 7A). Adjacent to the NE lateral margin is an area of highly discontinuous reflections, best expressed on the variance map in Fig. 7A. Some of these discontinuous reflections form lineations oriented oblique to the NE lateral margin. This area is also characterised by low-to-medium amplitude, discontinuous reflections at, and immediately beneath, the basal-shear surface (Fig. 7D). On top of the older MTC, there is a series of 0.5 to 1.5 km-long lineations that originate from, and trend at *c.*45^{o} to, the NE lateral margin (Figs. 7A and D).

The proximal part of the upper translation domain is dominated by debrite (SF-1) that surrounds scattered megaclasts (SF-4) (Fig. 7B). These megaclasts have elliptical to rectangular planview geometries, with long-axis lengths ranging from *c.*0.18 to 1 km and thicknesses of *c.*70 to 140 m (Fig. 7B). Seismic sections show that these megaclasts are sometimes internally folded and faulted (Fig. 7D). In the central part of this domain the megaclasts are concentrated and form *c.*15 km-long and 3 km-wide, convex-upslope cluster. This cluster is bound by a gradational boundary with SF-1 in the E, and an abrupt boundary in the W, the latter defined by the longitudinal shear zone (Fig. 7B). Most of the megaclast cluster occurs within Area A, although another cluster is observed *c.*5 km downdip to the N within Area B (Fig. 7B), with the two being separated by the longitudinal shear zone. Immediately downdip of the Area A megaclast cluster, a series convex-upslope bands are developed within the slides debritic matrix (Fig. 7B). These bands are sub-parallel to the overall, convex-upslope geometry of the cluster and to the long-axis of elongated clasts (Figs. 7B and 8A). In contrast, downdip from the eastern margin of the cluster, the bands show a convex-downslope geometry, terminating at the NE lateral margin (Figs. 7B and 8A). A NW-trending, narrow band (*c.*500 m-wide and *c.*10 km-long) debrite (SF-1) defines the boundary between these two sets of bands (Fig. 7B). There is a similar occurrence of convex-downslope bands downdip from the cluster in Area B (Fig. 9B).

Some of the features within the Gorgon Slide are expressed on its top surface (Fig. 7C). For example, the arcuate bands form ridges with positive seabed relief. These ridges terminate at the longitudinal shear zone between Areas A and B, abruptly changing their orientation (from convex-upslope to -downslope) at the internal shear zone (see Figs. 7C and 8).

Interpretation.– The converging-downslope geometry of the grooves implies that the pathway of the slide was focused towards the steep, NE lateral margin (Fig. 7A). As a result, the slide is thickest adjacent to this margin (see Fig. 3A). The pathway was likely controlled by the morphology of the basal-shear surface that broadly follows the morphology of the underlying substrate (see Fig. 4B). This supports the observations of Ortiz-Karpf et al. (2017), who stress the impact of seabed morphology on MTC emplacement. We interpret the pair of curved lineations as 'ramps' bounding an area called a 'flat' (Fig. 7A) (Trincardi and Argnani 1990; Lucente and Pini 2003; Frey-Martinez et al. 2005; Bull et al. 2009). The ramps record basal erosion by the overlying slide that are commonly expressed by truncated reflections of underlying substrate by a basal-shear surface (e.g. Bull et al. 2009). However, as the ramps in this domain represent relatively small steps (i.e. 10 m), the basal-shear surface does not truncate more than one reflector. We interpret the lineations oriented oblique to the NE lateral margin on, and immediately beneath, the basal-shear surface (Fig. 7A) as substrate that have undergone contractional deformation due to stress exerted by the passing slide, forming a 'basal-shear zone' (Butler and McCaffrey 2010; Hodgson et al. 2018; Cardona et al. 2020). Lineations on top of the older MTC (Fig. 7A) are interpreted as shear fractures (i.e. Riedel shears) that developed due to dextral strike-slip movement along the NE lateral margin as the Gorgon Slide translated northwestwards (e.g. Fleming and Johnson 1989; Martinsen 1994; Fossen 2016) (Fig. 7A). Fleming and Johnson (1989) suggest that this type of fractures is developed during an early stage of strike-slip faulting along lateral margin of the MTCs, prior to the formation of through-going lateral margins. They recorded fractures oriented at 45° clockwise from the trend of a dextral lateral margin, similar to the shear fractures found in our study.

The scattered megaclasts in the proximal part of this domain are clustered (see Fig. 7B), possibly due to downslope-convergence of material within the Gorgon Slide (see Fig. 7A). The clusters of megaclasts in Areas A and B are interpreted to have been initially emplaced as a single cluster. We interpret this cluster was subsequently cross-cut by the longitudinal shear zone (Figs. 7B and 8), with the formation and clustering of megaclasts inducing intra-slide velocity perturbations. These perturbations are evidenced by across-strike variations in the attitude of flow fabrics; i.e. convex-downslope flow fabrics in Areas A and B are located further downflow of the convex-upslope flow fabrics preserved immediately downdip, and perhaps in the strain shadow zone of, the major cluster of megaclasts in Area A (Figs. 7B and 8). Another indicator of internal velocity variation is the narrow area within Area A separating the convex-downslope and -upslope flow fabrics (Figs. 7B). The internal flow fabrics are expressed on the top surface of the MTC as ridges which are termed as secondary flow fabrics (Fig. 7C) (*sensu* Bull et al. 2009). This area is interpreted as an 'internal shear zone' (cf. Ogata et al. 2014; Bull and Cartwright 2019; Omeru and Cartwright 2019) that contains disaggregated material due to intense shearing. Other studies have also discussed how the entrainment and abrasion of megaclasts during transport of MTCs could affect flow rheology (e.g. Joanne et al. 2013; Ortiz-Karpf et al. 2017; Hodgson et al. 2018; Sobiesiak et al. 2019), and therefore variations in intra-MTC flow velocity.

Lower translation domain

Description.– On the basal-shear surface, the majority of kinematic indicators observed in the upper translation domain extend to this lower translation domain (i.e. ramp, deformed substrate and shear fractures; Fig. 9A). Grooves are, however, absent. Here, the ramps are deeper (*c.*20 m-deep, Fig. 9D), and lineations within the deformed substrate area are more apparent (Fig. 9A). Downflow from the deformed substrate are several SE-facing ramps (i.e. perpendicular to transport direction) that merge updip with the ramp extending downslope from the upper translation domain (Fig. 9A). NE of the deformed substrate, beyond the lateral margin and on top of the older MTC, are the downdip continuation of the N-trending shear fractures see in the upper translation domain. These fractures die-out downdip to the N.

Within the slide, area defined by the convex-upslope flow fabrics, bound between the longitudinal and internal shear zones within Area A, dies-out downslope (Fig. 9B). In contrast, the convex-downslope flow fabrics within Area B continue and are more prominent in this lower translation domain (Fig. 9B). Adjacent to the NE lateral margin, there is another cluster of megaclasts (Fig. 9B). In cross-section (Fig. 9D), this cluster contains megaclasts that have similar seismic expression to those in the upper translation domain (Figs. 7D and 8B-C). However, these megaclasts have shorter long-axes (*c.*0.05 to 0.54 km-long, compared to *c.*0.17 to 0.98 km-long) and are thicker (*c.*73 to 220 m, compared to *c.*70 to 137 m-thick) than those in the upper translation domain (see Fig. 10A). The long-axes trends of megaclasts in the upper (NNW) and lower (NE) translation domains also differ (Fig. 10B). We also identify megaclasts that are concentrated in the basal part of the slide ('basal megaclasts'; Fig. 9D): these are internally chaotic and transparent, but are defined by a folded, moderate-amplitude, relatively continuous reflections, and are underlain by a ramp.

The internal shear zone merges with the longitudinal shear zone in the distal part of the lower translation domain (Fig. 9C). These shear zones outline a downslope-narrowing area defined by convex-upslope ridges. Consequently, Area A becomes dominated by the convex-downslope ridges (Fig. 9C). However, immediately downflow from the point where the shear zones merge, the ridges in Area A have slightly convex-upslope geometries, most notably adjacent to the longitudinal shear zone (Fig. 9C).

Interpretation.– The ramps, deformed substrate, and shear fractures indicate that erosion and deformation also occurred in this lower translation domain (Fig. 9A). There is a close spatial relationship between the deformed substrate and the concentration of shear fractures (Fig. 9A), which also coincides with where the slide is thickest in Area A (Fig. 3A). This could imply that basal and lateral deformation of the substrate was more severe due to increased stress exerted by the passage of the thickest part of the Gorgon Slide. This contrasts with the interpretation of Cardona et al. (2020), who see no statistical correlation between the intensity of deformation of the basal-shear zone and the thickness of the overlying MTC.

The presence of longitudinal and internal shear zones suggest that internal variation of flow velocity identified in the upper translational domain also characterized the lower translational domain (Fig. 9B). Between these shear zones, the gradual downflow disappearance of the convex-upslope flow fabrics suggests a decrease in internal velocity perturbations induced by the cluster of megaclasts in the upper translation domain (Fig. 7B). The cluster of megaclasts adjacent to the NE lateral margin (Figs. 9B and D) is located immediately downflow from, and has a similar width (2.5 km) to, the deformed substrate area (Fig. 9A). Thus, basal and lateral deformation of the substrate expressed on the basal-shear surface (Fig. 9A) could be related in some way to this cluster of megaclasts, instead of reflecting the maximum thickness of the Gorgon Slide (Fig. 3A). This interpretation is supported by the same observation from the Rapanui MTD (Cardona et al. 2020), where the thickness of the deformed substrate is correlated to higher concentrations of rafted blocks (i.e. megaclasts), and not the thickness of overlying MTC. The higher concentration of megaclasts indicates an increase in flow competence overriding the area of the deformed substrate. In addition, the long-axis orientations of the megaclasts in the lower translation domain are generally oblique-to-sub-parallel to the overall north-westerly transport direction, which contrasts to those in the upper translation domain that are generally perpendicular to it (Fig. 10B). Their long-axis orientations are likely to be controlled by velocity gradients (Mazzanti and De Blasio 2010), where the megaclasts in the lower translation domain, adjacent to the NE lateral margin, were dragged against the stationary lateral wall (Fig. 9B). In contrast, the cluster of megaclasts in the upper translation domain, further away from the lateral margin, experienced a lower across-strike velocity gradient, meaning their long axis formed an overall convex-upslope geometry (Fig. 7B). The basal megaclasts appear more deformed than adjacent megaclasts (Fig. 9D), with their transparent internal seismic facies possibly recording intense shearing during transport (Alves 2015; Gamboa and Alves 2015). Their folded tops may be formed due to them impinging against the underlying ramp (Fig. 9D) (Jackson 2011).

The top surface supports the interpretation of kinematic indicators within the internal body of the slide (Figs. 9B-C). Here, it is also evident that velocity perturbation induced by the cluster of megaclasts in upper translation domain (Figs. 7B and 8A) had decreased, and diminished downflow, as clearly marked by the merging of the two shear zones (Fig. 9C). However, downflow from the point where these two merges, the presence of convex-upslope ridges within Area A (terminating at the longitudinal shear zone) suggests that internal velocity perturbations continued (Fig. 9C).

Toe domain

Description.– The basal-shear surface in this domain serves as the frontal margin of Area A, and swings through 90° to join the lateral margin of Area B that continues downdip, beyond the area imaged by 3D seismic reflection data (Fig. 11A). The seismic attributes expression of the deformed substrate (Fig. 11A) resembles that of the upper and lower translation domains (see Figs. 7A and 9A). In the SW part of this domain, there is a *c.*30 m-high ramp (Figs. 10A and D), which is of higher-relief than the one developed upslope in the lower translation domain (*c.*20 m).

Debrite (SF-1) and a fold-and-thrusts system (SF-3) dominate the distal part of Area A and B in the toe domain, respectively (Fig. 11B). The thrusts within Area B dip to the SE, sub-parallel to the transport direction of the slide (see Figs. 5G and 11B and D). Within the older MTC, there is a cluster of relatively large megaclasts (*c.*2.5 km-wide and *c.*5 km-long) that are deformed by NNW-SSE-striking, NE-dipping thrusts; these trend broadly perpendicular Area A's frontal margin and the NW-SE-striking thrusts within Area B (see Fig. 11B). Near the upper tips of these thrusts, the megaclasts are folded (see 'thrusted megaclasts' in Fig. 11D).

The toes region of Area A is defined by a rugose seabed characterized by *c.*30 m-high ridges that are elevated above the flat seabed capping the older MTC (see Fig. 11C). The vertical relief of the ridges in Area A is higher than in both Area B (*c.*10 m, Fig. 11C) and the lower translation domain (*c.*10 m, Fig. 9).

Interpretation.– The geometry of the basal-shear surface indicates that Area B extends further downdip than Area A (Fig. 11A). The deformed substrate and the ramp indicate that substrate deformation and erosion continued beneath the main body of the slide, despite being located further from the headwall.

Abrupt truncation of the thrusted megaclasts in the older MTC by the frontal margin of Area A, and the strike difference between thrusts within Area B and those in the megaclasts (Fig. 11B), indicate the thrusted megaclasts were emplaced in the older MTC, prior to the emplacement of the Gorgon Slide. Some thrusted megaclasts (i.e. indicated by high RMS amplitude) are observed within the frontal part of Area A (Fig. 11B). However, these thrusted megaclasts are distinctly different from those of the thrust system within Area B (Fig. 11D). This suggests that a few (older) thrusted megaclasts were only locally entrained by the Gorgon Slide in the very frontal part of the Area A (Fig. 11B). In contrast, no thrusted megaclasts were entrained along the NE lateral margin of Area B.

The longitudinal shear zone that extends from the upper translation domain (see Figs. 7A and 8A) joins Area B's lateral margin in the toe domain (Fig. 11B). This may indicate a relationship between the thrusted megaclasts in the older MTC and inferred intra-MTC velocity perturbation. Specifically, the velocity perturbation could have originated due to the passage of the Gorgon Slide onto (i.e. Area A), and partly around (i.e. Area B), the thrusted megaclasts in the older MTC, with this perturbation and subsequent arrest of the flow in Area A propagating upflow (Fig. 11B). Therefore, this velocity perturbation may have connected with the downflow-propagating velocity perturbation induced by the cluster of megaclasts in the upper translation domain (Figs. 7B and 8A). Frey-Martínez et al. (2006) also observed similar role of pre-existing megaclasts, where a single MTC flow bifurcates to form two flows with different transport directions.

The ridges at the frontal margin of Area A could indicate a buttressing effect of the slide against thrusted megaclasts in the older MTC (Fig. 11C), which then formed ridges that decrease in height upflow. In contrast, the ridges in Area B are of lower relief than those in Area A. Thus, the slide was not buttressed against the thrusted megaclasts and was able to translate further downdip (Fig. 11C).

Emplacement processes of the Gorgon Slide: a multi-cell flow emplacement mechanism

A multiple flow cell model for subaqueous slides is proposed by Alsop and Marco (2014) based on field data, developing a model originally proposed by Farrell (1984). They suggest that a large (first-order) MTC consists of a number of smaller (second-order) flow cells formed during the transport and ultimate emplacement of a sediment mass. These smaller flow cells may interact with each other and cause overprinting on earlier formed structures. Similar kinematic interactions between intra-flow cells are documented from sonar (e.g. Prior et al. 1984; Masson et al. 1993; Gee et al. 2001) and 3D seismic reflection data (e.g. Bull et al. 2009; Steventon et al. 2019), where primary (longitudinal shear zone) and secondary (sinuous flow fabrics) flow fabrics form between and define evolving cells (*sensu* Bull et al. 2009). These kinematic indicators suggest the portions (i.e. cells) of the translating mass were travelling at different speeds and/or travelled at slightly different times (Masson et al. 1993; Gee et al. 2005).

In this study, the Gorgon Slide appears to comprise at least two intra-MTC (second-order) flow cells. These are represented physically by Areas A and B, and for the purpose of this process-based interpretation are re-named as Cells A and B, respectively. The emplacement processes of the Gorgon Slide are captured in a schematic model that recognises three stages of development (Fig. 12).

Stage 1.– Prior to slope degradation, a surface rupture might have been triggered by two main mechanisms (Fig. 12A). First, the normal faults bounding the horst could have been inverted due to regional compression, which then destabilised the slope (Keep et al. 1998; Nugraha et al. 2019b). Second, the existence of pockmarks observed on the seabed (see Fig. 6) implies that there has been active fluid venting in the headwall area (Hengesh et al. 2013), most likely originating from the underlying, gas-bearing horst block hosting the Gorgon Field (Fig. 2). Gas leakage into shallower sediments could have lowered the shear strength of these sediments, and primed the slope for subsequent failure (Scarselli et al. 2013). However, the Gorgon Slide was not an isolated occurrence, but rather the most recent. Previous collapse of the continental margin is recorded in the older (pre-Gorgon) MTC, most notably, the thrusted megaclasts that had already been emplaced in the vicinity of the future toe domain of the Gorgon Slide (Fig. 12A).

Stage 2.– The arcuate geometry of the main headwall scarp indicates that the failed sediments were evacuated during a single mass-transport event (see Fig. 6). The evacuated sediments might include megaclasts derived from either the headwall and/or megaclasts entrained from the layered slope substrate (Figs. 11B and 4A). During translation, the megaclasts were deformed and fragmented (e.g. Gee et al. 2005; Alves 2015).

The downslope-converging grooves within the headwall and upper translation domains suggest a convergent pathway of the slide, resulting in the clustering of the megaclasts (Fig. 12B). In the lee-side of the cluster of megaclasts, the following features formed: (i) convex-upslope flow fabrics within the slide, and (ii) convex-upslope ridges on top of the slide. These features indicate slower transport velocity in and around the area of concentrated megaclasts (Fig. 12B). Higher transport velocities of flows moving around the megaclast-rich area led to the formation of the longitudinal shear zone, and the initiation of Cells A and B. The cluster of megaclasts effectively acted as an obstacle to the initial, single-cell flow. Other studies have also documented such mechanism, where the geometry of flow fabrics and ridges downslope from translating megaclasts suggest slower-moving flows than surrounding materials (e.g. Masson et al. 1993; Lastras et al. 2005; Gee et al. 2006; Bull et al. 2009).

Stage 3.– The downslope propagation of the basal-shear surface was coupled with the evolution of the internal body and top surface of the slide. The area covering the convex-upslope flow fabrics and ridges narrowed downslope (Fig. 12C), which suggests a reduction in the influence of the cluster of megaclasts on slowing down the flow of material in its lee-side. Thus, we interpret this area as a 'shadow zone'. The shadow zone is bound by the longitudinal shear zone separating the two cells, and the internal shear zone within Cell A (Fig. 12C). The formation of this shadow zone and related bounding structures illustrates how megaclasts influence flow processes within an MTC (e.g. Masson et al. 1993; Lucente and Pini 2003; Jackson 2011; Hodgson et al. 2018).

Downflow from the shadow zone, ridges within Cell A show convex-upslope geometries adjacent to the longitudinal shear zone. In contrast, ridges within Cell B consistently exhibit convex-downslope geometries (Fig. 12C). These geometries indicate that Cell A resisted the downslope translation of Cell B, meaning its internal ridges were dragged downslope whereas those in Cell B were dragged upslope (Fig. 12C). Therefore, we suggest that Cell A was travelling more slowly than Cell B. Furthermore, the prominent seabed relief characterizing the frontal margin of Cell A suggest a shortening and thickening effect driven by this part of the flow being buttressed against pre-existing thrusted megaclasts in the older MTC (Fig. 12C) (Masson et al. 1993; Gee et al. 2006). Cell B, however, was able to translate further downdip than Cell A, meaning the former travelled faster and further than the latter.

Single versus multiple failure events.– Limited spatial resolution of even high-quality seismic reflection data indicates the challenge in determining whether an apparently singular sedimentary body (i.e. the Gorgon Slide) was emplaced by one or multiple failure events. We interpret that the Gorgon Slide was deposited by a single failure event, rather than several discrete events, based on: (i) the lack of cross-cutting grooves on the basal shear surface in the headwall (Fig. 6) and upper translation domains (Fig. 7A); (ii) the shear zones (e.g. Figs. 5D-E), internal thrusts (e.g. Fig. 5G), and megaclasts (Fig. 8B) span the entire height of the slide; (iii) there is no seismically resolvable evidence for intra-deposit hemipelagic (or similar) deposits that might represent even brief hiatuses between more rapid, catastrophic, MTC-related deposition, such as the paleo-seabed on top of the older MTC (e.g. Fig. 4B); (iv) the lateral margin and longitudinal shear zone can be mapped, without abrupt discontinuities, across considerable widths of the slide (e.g. Fig. 3B); (v) the observed shadow zone and associated flow fabrics (Figs. 8B and 12C) could only be formed due to interactions between a single mass failure and flow obstacles; and (vi) the present-day seabed relief show distinct characteristics, where the seabed on top of the older MTC is smooth and the top of the Gorgon Slide is highly rugose (Figs. 3B and 4B).

DISCUSSION

Impact of flow cell formation on MTC kinematics and structure

Submarine debris flows can travel for tens to hundreds of km across low gradient (*c.*<1^{o}) continental slopes, despite their cohesive nature (Gee et al. 1999; Lastras et al. 2005). This mobility can be explained by sustained pore-fluid pressure within the flow during transport (Major and Iverson 1999; McArdell et al. 2007), and the presence of a thin lubricating layer of fluid at the base of the frontal part of the flow (i.e. hydroplaning, Mohrig et al. 1998). Ultimately, a debrite is formed by *en masse* freezing of the debris flow (e.g. Talling et al. 2012), where materials at flow margins (i.e. frontal and lateral) cease moving first, followed by materials in the main body of the flow (Iverson 1997).

The Gorgon Slide provides evidence of a mass flow splitting into two smaller flow cells (Cell A and B, Fig. 12). The relationship between the two cells suggests that Cell A ceased movement, while Cell B was still in motion. This suggests that *en masse* freezing did not occur across the entire body of the flow synchronously. Instead, individual flow cells froze at different times, resulting in different runout duration and distance of the cells. We propose that lateral friction and related pore-fluid pressure played an important role in controlling the runout distance of the two cells, in addition to the presence of pre-existing thrusted megaclasts. The longitudinal shear zone may have sustained excess pore-fluid pressure between the two cells, such that low friction between the two cells could be maintained, allowing continued translation of Cell B despite being partly impeded by Cell A. In contrast, pore-fluid pressure was likely dissipated at the lateral margins of the flow during translation (e.g. NE lateral margin, Fig. 3), resulting in relatively high friction between the moving slide (e.g. Cell A) and stationary lateral substrate (i.e. the older MTC and locally other slope strata). This high friction at the lateral margin was likely to reduce runout distance more significantly than the friction at the longitudinal shear zone. Such mechanisms are also observed from experimental studies (Major and Iverson 1999; De Haas et al. 2015).

Our results suggest that a multi-cell debris flow could undergo 'punctuated' freezing, where one cell may have a shorter runout distance than the others due to spatial differences in the pore pressure and related friction between bounding cells. The flow behaviour documented in our study may be considered for modelling the potential impact of MTCs on subsea infrastructure. For example, cell and shear zone formation, and the presence of pre-existing megaclasts and barriers to flow translation, may result in variable shear and stresses being exerted on seabed pipelines.

Controls on flow cell formation

Flow cell formation within an MTC depends on internal velocity perturbations, which are controlled by variations in at least three local factors (Farrell 1984; Alsop and Marco 2011; Alsop and Marco

2014): (i) the lithology and/or geometry of stratigraphic elements overridden by the MTC (e.g. older MTCs, channels and lobes); (ii) fluid pressures within the MTC and/or its substrate and lateral margins; and (iii) the slope gradient and/or geometry of basal-shear surface underlying the MTC.

In the Gorgon Slide, a cluster of megaclasts within a debritic matrix-initiated flow cell formation. This implies that lithology, in particular variations of the degree of disaggregation within the slide, play a key role in forming the two seismic-scale flow cells. In addition, the geometry of the basal-shear surface was also important, given it caused the flow to converge, clustering the megaclasts, initiating velocity perturbation, and terminating the flow cells. These three local variations may have been influential prior to emplacement, but their properties could also evolve during translation and cessation of the parent flow (Iverson 1997; Dykstra et al. 2011; Joanne et al. 2013; Alsop and Marco 2014; Ortiz-Karpf et al. 2017; Hodgson et al. 2018).

Origin of the pre-existing thrusted megaclasts

We have established that the thrusted megaclasts were emplaced within an older MTC, and, thus, had existed in their present position prior to emplacement of the Gorgon Slide. Here, we discuss possible origins of the thrusted megaclasts, notably whether they are *in-situ* (remnant) or were translated?

Relatively continuous, sub-parallel reflections at the base of the thrusted megaclasts could support an *in-situ* origin (Fig. 11D). However, the NE-dipping thrusts originating from the base, and folded reflections toward the top, of the megaclasts, imply contractional strain as a result of broadly NE-SW trending σ_1 stress (Fig. 11D). It is unlikely this stress was exerted by the Gorgon Slide, given this body was being transported towards the NW. It is similarly unlikely that the NE-dipping thrusts were formed in response to south-westwards translation of the older MTC, given there is no possible MTC source area located towards the NE (see location of the NW Australian shelf, Fig. 1A).

If the thrusted megaclasts were to be deformed within or translated by an MTC, this MTC was likely sourced either from (i) the Exmouth Plateau Arch (i.e. to the SW from the megaclasts), or (ii) the NW Shelf of Australia (see Fig. 1A). As the thrusts of the megaclasts are NE-dipping (Fig. 11D), the megaclasts are unlikely to be deformed or translated by a NE-flowing MTC originated from the arch; such an MTC would likely produce SW-dipping thrusts. Thus, the MTC forming the thrusted megaclasts was more likely sourced from the NW Shelf (i.e. similar to the Gorgon Slide). However, a NW-flowing MTC should generate SE-dipping rather than NE-dipping thrusts, thus we propose that the megaclasts were shortened during translation within the NW-flowing MTC within a locally contractional strain field near a basal shear surface ramp, and subsequently rotated counter-clockwise (*c.*70-80^{o}) before coming to rest at their present location. A similar process has been documented in other studies, such as in Storegga Slide, where megaclasts were re-oriented from perpendicular to become sub-parallel to transport direction with increasing distance from headwall scarp (Bull et al. 2009).

CONCLUSIONS

This interpretation of a 3D seismic reflection dataset, investigating the emplacement of a recent mass-transport complex (MTC), the Gorgon Slide (Exmouth Plateau, offshore NW Australia), concludes that:

1. The Gorgon Slide was evacuated from a steep, NE-SW trending, *c.*350 m-high headwall scarp and transported towards the NW. Layered slope strata in this headwall domain are the likely source of megaclasts that are subsequently transported downslope.
2. In the proximal part of the translation domain, downslope-converging grooves on the basal-shear surface indicate that the pathway of the slide was focused towards its lateral margin in the NE. The convergent pathway of the flow results in the clustering of the megaclasts, whose long-axes are generally trending NE-SW, perpendicular to the transport direction. This clustering of megaclasts became an obstacle to flow, causing velocity perturbation within the slide. The velocity perturbation is recorded by convex-upslope flow fabrics within the internal body, and by convex-upslope ridges on the seabed. These features indicate a slower transport

velocity of the cluster of megaclasts and materials in its lee-side. The area of the slower-moving material narrows downslope, indicating that velocity perturbation caused by the cluster of megaclasts gradually diminished downflow, forming a 'shadow zone'. Transport velocities of flows were higher around the megaclasts, resulting in the formation of longitudinal shear zones and the initiation of two flow cells, namely Cells A and B.

3. The distal part of the translation domain contains kinematic indicators recording erosional and deformational processes on the basal-shear surface. Erosional processes are evidenced by a ramp, and deformational processes are evidenced by deformed substrate or basal-shear zone and shear fractures adjacent to the NE lateral margin. The deformed substrate and shear fractures are closely related to the thickest part of the slide, comprising a cluster of megaclasts, with individual megaclasts generally trending NNW-SSE, oblique to sub-parallel to the transport direction. Flow fabrics within the slide and ridges on the seabed of Cell A were dragged downslope, while those of Cell B were dragged upslope. This points to Cell A acting as an impediment to the movement of the faster-moving Cell B.
4. In the toe domain, the frontal margin of Cell A is marked by positive seabed relief (*c.*30 m-high) that gradually decreases upflow, which is significantly higher than the relief of Cell B (*c.*10 m-high). This suggests that Cell A was buttressed against a pre-existing cluster of megaclasts (i.e. encased by older MTC), while Cell B was not. Therefore, as there were no flow obstacles, Cell B was able to travel further than Cell A.
5. The morphology of the basal-shear surface and the degree of disaggregation within the slide, especially the megaclasts, played important roles in flow cell evolution. The basal-shear surface controlled the pathway of the slide, and the clustering of the megaclasts. The megaclast clusters induced internal velocity perturbations that controlled the initiation and cessation of intra-MTC flow cells.
6. Simultaneous *en masse* freezing was unlikely to have occurred throughout the body of the Gorgon Slide. Instead, 'punctuated' freezing, where motion in Cell A had ceased while Cell B

was still active, occurred due to differential friction and pore-fluid pressure dissipation at flow cells margins. For instance, excess pore-fluid can be maintained within the longitudinal shear zone, so that Cell B only experienced minimal friction against the Cell A. In contrast, excess pore-fluid pressure was likely to dissipate at lateral margins, such as at the NE lateral margin separating Cell A and stationary substrate. Thus, Cell A experienced higher lateral friction than that of Cell B, resulting in reduced runout distance. This punctuated freezing mechanism may be considered for modelling the impact of MTCs on submarine infrastructures.

ACKNOWLEDGEMENTS

We thank Geoscience Australia for providing seismic and borehole data. Schlumberger and Geoteric are thanked for providing software licenses to Imperial College London. The first author thanks the Indonesia Endowment Fund for Education (LPDP) (Grant No.: 20160822019161) for its financial support.

CONFLICT OF INTEREST

No conflict of interest declared.

REFERENCES

Alsop, G.I., and Marco, S., 2011, Soft-sediment deformation within seismogenic slumps of the Dead Sea Basin: Journal of Structural Geology, v. 33, p. 433-457.

Alsop, G.I., and Marco, S., 2014, Fold and fabric relationships in temporally and spatially evolving slump systems: A multi-cell flow model: Journal of Structural Geology, v. 63, p. 27-49.

Alves, T.M., Kurtev, K., Moore, G.F., and Strasser, M., 2014, Assessing the internal character, reservoir potential, and seal competence of mass-transport deposits using seismic texture: A geophysical and petrophysical approach: AAPG Bulletin, v. 98, p. 793-824.

Alves, T.M., 2015, Submarine slide blocks and associated soft-sediment deformation in deep-water basins: A review: Marine and Petroleum Geology, v. 67, p. 262-285.

Apthorpe, M., 1988, Cainozoic depositional history of the North West Shelf: The North West Shelf, Australia: Petroleum Exploration Society of Australia, p. 55-84.

Boyd, R., Williamson, P., and Haq, B., 1993, Seismic Stratigraphy and Passive-Margin Evolution of the Southern Exmouth Plateau, *in* Posamentier, H.W., Summerhayes, C.P., Haq, B.U., and Allen, G.P., eds., Sequence Stratigraphy and Facies Associations: Oxford, Blackwell Scientific Publications, p. 579-603.

Brown, A.R., 2011, Interpretation of three-dimensional seismic data: AAPG Memoir 42, SEG Investigations in Geophysics No. 9: Tulsa, The American Association of Petroleum Geologists and the Society of Exploration Geophysicists.

Bull, S., Cartwright, J., and Huuse, M., 2009, A review of kinematic indicators from mass-transport complexes using 3D seismic data: Marine and Petroleum Geology, v. 26, p. 1132-1151.

Bull, S., and Cartwright, J.A., 2019, Line length balancing to evaluate multi-phase submarine landslide development: an example from the Storegga Slide, Norway: Geological Society, London, Special Publications, v. 500.

Butler, R., and McCaffrey, W., 2010, Structural evolution and sediment entrainment in mass-transport complexes: outcrop studies from Italy: Journal of the Geological Society, v. 167, p. 617-631.

Cardona, S., Wood, L.J., Dugan, B., Jobe, Z., and Strachan, L.J., 2020, Characterization of the Rapanui mass-transport deposit and the basal shear zone: Mount Messenger Formation, Taranaki Basin, New Zealand: Sedimentology, v. 67, p. 2111-2148.

Cathro, D.L., Austin Jr, J.A., and Moss, G.D., 2003, Progradation along a deeply submerged OligoceneMiocene heterozoan carbonate shelf: How sensitive are clinoforms to sea level variations?: AAPG bulletin, v. 87, p. 1547-1574.

Chopra, S., and Marfurt, K.J., 2007, Seismic attributes for prospect identification and reservoir characterization, v. 11, Society of Exploration Geophysicists Tulsa, Oklahoma.

Clegg, L., Sayers, M., and Tait, A., 1992, The Gorgon Gas Field: Chapter 32, p. 517-518.

De Haas, T., Braat, L., Leuven, J.R., Lokhorst, I.R., and Kleinhans, M.G., 2015, Effects of debris flow composition on runout, depositional mechanisms, and deposit morphology in laboratory experiments: Journal of Geophysical Research: Earth Surface, v. 120, p. 1949-1972.

Dott, R., 1963, Dynamics of subaqueous gravity depositional processes: AAPG Bulletin, v. 47, p. 104-128.

Dykstra, M., Garyfalou, K., Kertznus, V., Kneller, B., Milana, J.P., Molinaro, M., Szuman, M., and Thompson, P., 2011, Mass-transport deposits: Combining outcrop studies and seismic forward modeling to understand lithofacies distributions, deformations, and their seismic stratigraphic expression: SEPM Special Publication, v. 96, p. 293-310.

Eckersley, A.J., Lowell, J., and Szafian, P., 2018, High-definition frequency decomposition: Geophysical Prospecting, v. 66, p. 1138-1143.

Farrell, S.G., 1984, A dislocation model applied to slump structures, Ainsa Basin, South Central Pyrenees: Journal of Structural Geology, v. 6, p. 727-736.

Fisher, R.V., 1983, Flow transformations in sediment gravity flows: Geology, v. 11, p. 273-274.

Fleming, R.W., and Johnson, A.M., 1989, Structures associated with strike-slip faults that bound landslide elements: Engineering Geology, v. 27, p. 39-114.

Fossen, H., 2016, Structural geology, Cambridge University Press.

FREY-MARTINEZ, J., CARTWRIGHT, J., AND HALL, B., 2005, 3D seismic interpretation of slump complexes: examples from the continental margin of Israel: Basin Research, v. 17, p. 83-108.

FREY-MARTÍNEZ, J., CARTWRIGHT, J., AND JAMES, D., 2006, Frontally confined versus frontally emergent submarine landslides: A 3D seismic characterisation: Marine and Petroleum Geology, v. 23, p. 585-604.

GAMBOA, D., ALVES, T., CARTWRIGHT, J., AND TERRINHA, P., 2010, MTD distribution on a 'passive' continental margin: The Espírito Santo Basin (SE Brazil) during the Palaeogene: Marine and Petroleum Geology, v. 27, p. 1311-1324.

GAMBOA, D., AND ALVES, T.M., 2015, Three-dimensional fault meshes and multi-layer shear in mass-transport blocks: Implications for fluid flow on continental margins: Tectonophysics, v. 647, p. 21-32.

GEE, M., MASSON, D., WATTS, A., AND ALLEN, P., 1999, The Saharan debris flow: an insight into the mechanics of long runout submarine debris flows: Sedimentology, v. 46, p. 317-335.

GEE, M., GAWTHORPE, R., AND FRIEDMANN, J., 2005, Giant striations at the base of a submarine landslide: Marine Geology, v. 214, p. 287-294.

GEE, M., GAWTHORPE, R., AND FRIEDMANN, S., 2006, Triggering and evolution of a giant submarine landslide, offshore Angola, revealed by 3D seismic stratigraphy and geomorphology: Journal of Sedimentary Research, v. 76, p. 9-19.

GEE, M.J., MASSON, D.G., WATTS, A.B., AND MITCHELL, N.C., 2001, Passage of debris flows and turbidity currents through a topographic constriction: seafloor erosion and deflection of flow pathways: Sedimentology, v. 48, p. 1389-1409.

GOLOVCHENKO, X., BORELLA, P.E., AND O'CONNELL, S.B., 1992, Sedimentary cycles on the Exmouth Plateau, *in* Von Rad, U., Haq, B.U., Kidd, R.B., and O'Connell, S.B., eds., Proceedings of the Ocean Drilling Program, Scientific Results: College Station, TX, Ocean Drilling Program, p. 279-291.

Hengesh, J.V., Dirstein, J.K., and Stanley, A.J., 2013, Landslide geomorphology along the Exmouth Plateau continental margin, North West Shelf, Australia: Australian Geomechanics, v. 48, p. 71-92.

Hodgson, D., Brooks, H., Ortiz-Karpf, A., Spychala, Y., Lee, D., and Jackson, C.-L., 2018, Entrainment and abrasion of megaclasts during submarine landsliding and their impact on flow behaviour: Geological Society, London, Special Publications, v. 477, p. SP477. 26.

Hull, J.N.F., and Griffiths, C.M., 2002, Sequence stratigraphic evolution of the Albian to Recent section of the Dampier Sub-basin, NorthWest Shelf, Australia: The Sedimentary Basins of Western Australia 3: Proceedings of the Petroleum Exploration Society of Australia Symposium, p. 617-639.

Iverson, R.M., 1997, The physics of debris flows: Reviews of geophysics, v. 35, p. 245-296.

Jackson, C.A., 2011, Three-dimensional seismic analysis of megaclast deformation within a mass transport deposit; implications for debris flow kinematics: Geology, v. 39, p. 203-206.

Joanne, C., Lamarche, G., and Collot, J.Y., 2013, Dynamics of giant mass transport in deep submarine environments: the Matakaoa Debris Flow, New Zealand: Basin Research, v. 25, p. 471-488.

Keep, M., Powell, C., and Baillie, P., 1998, Neogene deformation of the North West Shelf, Australia: The sedimentary basins of Western Australia, v. 2, p. 81-91.

Lastras, G., De Blasio, F.V., Canals, M., and Elverhøi, A., 2005, Conceptual and numerical modeling of the BIG'95 debris flow, western Mediterranean Sea: Journal of Sedimentary Research, v. 75, p. 784-797.

Longley, I.M., Buessenschuett, C., Clydsdale, L., Cubitt, C.J., Davis, R.C., Johnson, M.K., Marshall, N.M., Murray, A.P., Somerville, R., and Spry, T.B., 2002, The North West Shelf of Australia - a Woodside Perspective, *in* Keep, M., and Moss, S.J., eds., The Sedimentary Basins of Western Australia 3: Petroleum Exploration Society of Australia Symposium: Perth, p. 28-88.

Lucente, C.C., and Pini, G.A., 2003, Anatomy and emplacement mechanism of a large submarine slide within a Miocene foredeep in the northern Apennines, Italy: A field perspective: American Journal of Science, v. 303, p. 565-602.

Major, J.J., and Iverson, R.M., 1999, Debris-flow deposition: Effects of pore-fluid pressure and friction concentrated at flow margins: Geological Society of America Bulletin, v. 111, p. 1424-1434.

Martinsen, O., 1994, Mass movements, The geological deformation of sediments, Springer, p. 127-165.

Masson, D., Huggett, Q., and Brunsden, D., 1993, The surface texture of the Saharan debris flow deposit and some speculations on submarine debris flow processes: Sedimentology, v. 40, p. 583-598.

Masson, D., Harbitz, C., Wynn, R., Pedersen, G., and Løvholt, F., 2006, Submarine landslides: processes, triggers and hazard prediction: Philosophical Transactions of the Royal Society A: Mathematical, Physical and Engineering Sciences, v. 364, p. 2009-2039.

Mazzanti, P., and De Blasio, F., 2010, Peculiar morphologies of subaqueous landslide deposits and their relationship to flow dynamics, Submarine mass movements and their consequences, Springer, p. 141-151.

McArdell, B.W., Bartelt, P., and Kowalski, J., 2007, Field observations of basal forces and fluid pore pressure in a debris flow: Geophysical research letters, v. 34.

McCormack, K., and McClay, K., 2013, Structural Architecture of the Gorgon Platform, North West Shelf, Australia: The Sedimentary Basins of Western Australia IV: Proceedings of the Petroleum Exploration Society of Australia Symposium, Perth, WA, p. 24.

McGilvery, T.A.H., Geoffrey, 2004, Seafloor and shallow subsurface examples of mass transport complexes, Offshore Brunei, Offshore Technology Conference: Houston.

Mohrig, D., Ellis, C., Parker, G., Whipple, K.X., and Hondzo, M., 1998, Hydroplaning of subaqueous debris flows: Geological Society of America Bulletin, v. 110, p. 387-394.

MOSCARDELLI, L., AND WOOD, L., 2008, New classification system for mass transport complexes in offshore Trinidad: Basin Research, v. 20, p. 73-98.

MOSS, G.D., CATHRO, D.L., AND AUSTIN, J.A., 2004, Sequence biostratigraphy of prograding clinoforms, northern Carnarvon Basin, Western Australia: a proxy for variations in Oligocene to Pliocene global sea level?: Palaios, v. 19, p. 206-226.

NARDIN, T.R., HEIN, F., GORSLINE, D.S., AND EDWARDS, B., 1979, A review of mass movement processes sediment and acoustic characteristics, and contrasts in slope and base-of-slope systems versus canyon-fan-basin floor systems: SEPM Special Publication, v.27, p. 61-73.

NEMEC, W., 1991, Aspects of sediment movement on steep delta slopes, *in* Colella, A., and Prior, D.B., eds., Coarsed-Grained Deltas, International Association of Sedimentologists, p. 29-73.

NUGRAHA, H.D., JACKSON, C.A.-L., JOHNSON, H.D., HODGSON, D.M., AND CLARE, M., 2019a, How erosive are submarine landslides?, EarthArXiv.

NUGRAHA, H.D., JACKSON, C.A., JOHNSON, H.D., HODGSON, D.M., AND REEVE, M.T., 2019b, Tectonic and oceanographic process interactions archived in Late Cretaceous to Present deep-marine stratigraphy on the Exmouth Plateau, offshore NW Australia: Basin Research, v. 31, p. 405-430.

OGATA, K., MOUNTJOY, J., PINI, G.A., FESTA, A., AND TINTERRI, R., 2014, Shear zone liquefaction in mass transport deposit emplacement: a multi-scale integration of seismic reflection and outcrop data: Marine Geology, v. 356, p. 50-64.

OMERU, T., AND CARTWRIGHT, J.A., 2019, The efficacy of kinematic indicators in a complexly deformed Mass Transport Deposit: Insights from the deepwater Taranaki Basin, New Zealand: Marine and Petroleum Geology, v. 106, p. 74-87.

ORTIZ-KARPF, A., HODGSON, D.M., JACKSON, C.A.-L., AND MCCAFFREY, W.D., 2017, Influence of Seabed Morphology and Substrate Composition On Mass-Transport Flow Processes and Pathways: Insights From the Magdalena Fan, Offshore Colombia: Journal of Sedimentary Research, v. 87, p. 189-209.

Parker, E.J., Traverso, C.M., Moore, R., Evans, T., and Usher, N., 2008, Evaluation of landslide impact on deepwater submarine pipelines, Offshore technology conference: Houston.

Partyka, G., Gridley, J., and Lopez, J., 1999, Interpretational applications of spectral decomposition in reservoir characterization: The Leading Edge, v. 18, p. 353-360.

Posamentier, H.W., and Kolla, V., 2003, Seismic geomorphology and stratigraphy of depositional elements in deep-water settings: Journal of Sedimentary Research, v. 73, p. 367-388.

Posamentier, H.W., and Martinsen, O.J., 2011, The character and genesis of submarine mass-transport deposits: insights from outcrop and 3D seismic data: Mass-transport deposits in deepwater settings: Society for Sedimentary Geology (SEPM) Special Publication 96, p. 7-38.

Prélat, A., Pankhania, S.S., Jackson, C.A.-L., and Hodgson, D.M., 2015, Slope gradient and lithology as controls on the initiation of submarine slope gullies; Insights from the North Carnarvon Basin, Offshore NW Australia: Sedimentary Geology, v. 329, p. 12-17.

Prior, D.B., Bornhold, B., and Johns, M., 1984, Depositional characteristics of a submarine debris flow: The Journal of Geology, v. 92, p. 707-727.

Randolph, M.F., and White, D.J., 2012, Interaction forces between pipelines and submarine slides—A geotechnical viewpoint: Ocean Engineering, v. 48, p. 32-37.

Sawyer, D.E., Flemings, P.B., Dugan, B., and Germaine, J.T., 2009, Retrogressive failures recorded in mass transport deposits in the Ursa Basin, Northern Gulf of Mexico: Journal of Geophysical Research: Solid Earth, v. 114.

Scarselli, N., McClay, K., and Elders, C., 2013, Submarine slide and slump complexes, Exmouth Plateau, NW Shelf of Australia: The Sedimentary Basins of Western Australia IV: Proceedings of the Petroleum Exploration Society of Australia Symposium.

Sobiesiak, M.S., Kneller, B., Alsop, G.I., and Milana, J.P., 2018, Styles of basal interaction beneath mass transport deposits: Marine and Petroleum Geology, v. 98, p. 629-639.

Sobiesiak, M.S., Buso, V.V., Kneller, B., Alsop, G.I., and Milana, J.P., 2019, Block Generation, Deformation, and Interaction of Mass-Transport Deposits With the Seafloor: An Outcrop-

Based Study of the Carboniferous Paganzo Basin (Cerro Bola, NW Argentina): Submarine Landslides: Subaqueous Mass Transport Deposits from Outcrops to Seismic Profiles, p. 91-104.

Steventon, M.J., Jackson, C.A., Hodgson, D.M., and Johnson, H.D., 2019, Strain analysis of a seismically imaged mass-transport complex, offshore Uruguay: Basin Research, v. 31, p. 600-620.

Sun, Q., Alves, T., Lu, X., Chen, C., and Xie, X., 2018, True volumes of slope failure estimated from a Quartenary mass-transport deposit in the northern South China Sea: Geophysical Research Letters, v. 45, p. 2642-2651.

Talling, P.J., Masson, D.G., Sumner, E.J., and Malgesini, G., 2012, Subaqueous sediment density flows: Depositional processes and deposit types: Sedimentology, v. 59, p. 1937-2003.

Tindale, K., Newell, N., Keall, J., and Smith, N., 1998, Structural evolution and charge history of the Exmouth Sub-basin, Northern Carnarvon Basin, Western Australia, *in* Purcell, P.G., and Purcell, R.R., eds., The Sedimentary Basins of Western Australia 2: Proceedings of the Petroleum Exploration Society of Australia: Perth, p. 473-490.

Trincardi, F., and Argnani, A., 1990, Gela submarine slide: a major basin-wide event in the Plio-Quaternary foredeep of Sicily: Geo-Marine Letters, v. 10, p. 13.

Vanneste, M., Forsberg, C.F., Glimsdal, S., Harbitz, C.B., Issler, D., Kvalstad, T.J., Løvholt, F., and Nadim, F., 2013, Submarine landslides and their consequences: what do we know, what can we do?, Landslide science and practice, Springer, p. 5-17.

Varnes, D.J., 1978, Slope movement types and processes: Special report, v. 176, p. 11-33.

Weimer, P., and Shipp, C., 2004, Mass Transport Complexes: Musing on past uses and suggestions for future directions, Offshore Technology Conference: Houston.

Zakeri, A., 2009, Review of state-of-the-art: Drag forces on submarine pipelines and piles caused by landslide or debris flow impact: Journal of offshore mechanics and Arctic engineering, v. 131.

Zeng, H., Henry, S.C., and Riola, J.P., 1998, Stratal slicing, Part II: Real 3-D seismic data: Geophysics, v. 63, p. 514-522.

FIGURE CAPTIONS

Fig. 1.--- A) Location of the study area. Regional seismic line (orange) across several wells (see Fig. 2). **B)** Seabed map of the Gorgon Slide, and industry well data (red dots) available for this study. The Gorgon Slide is expressed as rugose relief on the seabed. Both evacuation and most of deposition zones are imaged within the 3D seismic reflection data. **C)** Outline of the deposits of the Gorgon Slide (dark grey), where a minor area (*c.*7%) of the total slide area in the NW (dashed line) is not imaged within the 3D seismic reflection data. This minor part is delineated using 2D seismic lines (green). Five 3D seismic reflection datasets (Gorgon, Acme, Draeck, Duyfken, and Io-Jansz) were used in this study. Bathymetry and topography data are from Geoscience Australia.

Fig. 2.--- A regional seismic section across the Exmouth Plateau (see Fig. 1 for location). **A)** Uninterpreted. **B)** Interpreted. The Gorgon Slide is bound by a basal-shear surface (yellow) at the base and seabed (blue) at the top. Modified from Nugraha et al. (2019b).

Fig. 3.--- A) Thickness map of the Gorgon Slide showing lateral boundaries of the slide (i.e. NE lateral margin and pinch-out in the SW), with thickness concentration adjacent to the NE lateral margin. We divide rugged geometry of the frontal margin into eastern and western frontal margins. **B)** Seabed dip map showing two distinct sub-bodies (namely Area A and B) within the slide. The two areas are separated by a zone of longitudinal shear. The depositional zone of the slide comprises upper (UTD) and lower (LTD) translation and toe domains. **C)** A 3D perspective of seabed structure map in the LTD showing the geometry of the longitudinal shear zone.

Fig. 4.--- A) Dip-oriented seismic section across the Gorgon Slide showing the headwall scarp, evacuation and deposition zones. **B)** Strike-oriented seismic section showing the asymmetric geometry of the slide, with erosional lateral margin in the NE and pinch-out in the SW.

Fig. 5.--- Seismic facies classification used in this study. **A)** Seismic facies description and interpretation. **B)** Variance attributes extraction between the basal-shear surface and an iso-

proportional surface (50% between the basal-shear surface and the seabed). **C-E)** Seismic sections showing seismic facies within the translation domain. **F)** A time-slice of variance attribute extraction (see G for position) showing seismic facies in the toe domain. **G)** A seismic section showing seismic facies in the toe domain. Vertical exagerration of all seismic sections is 15.

Fig. 6.--- Seabed map showing kinematic indicators in the headwall domain, which include the main headwall of the Gorgon Slide, grooves, crown cracks, pockmarks, and a small scarp. **A)** Uninterpreted. **B)** Interpreted.

Fig. 7.--- Upper translation domain of the Gorgon Slide. **A)** Basal-shear surface variance map (top) and its interpretation (bottom). **B)** Internal body RMS amplitude map (extracted 50 ms above and below isoproportional horizon, orange) (top) and its interpretation (bottom). **C)** Top surface dip map (top) and its interpretation (bottom). **D)** Seismic sections, uninterpreted (above) and interpreted (bottom), showing seismic facies across the upper translation domain. See text for discussions.

Fig. 8.--- A) Spectral decomposition map within the slide (50% between basal-shear and top surfaces) showing features within upper translation domain in detail. **B)** Uninterpreted, and **C)** interpreted, seismic section along megaclasts (SF-4) across Area A and B. See text for discussion.

Fig. 9.--- Lower translation domain of the Gorgon Slide. **A)** Basal-shear surface variance map (top) and its interpretation (bottom). **B)** Internal body RMS amplitude map (extracted 50 ms above and below isoproportional horizon, orange) (top) and its interpretation (bottom). **C)** Top surface dip map (top) and its interpretation (bottom). **D)** Seismic sections, uninterpreted (above) and interpreted (bottom), showing seismic facies across the upper translation domain. See text for discussion.

Fig. 10.--- Dimensions and orientation of the megaclasts in the upper and translation domains. **A)** Megaclasts in the upper translation domain are generally thinner with longer long-axes, as compared to the ones in the lower translation domain that are thicker with shorter long-axes. **B)** Megaclasts in

the upper translation domain are generally oriented perpendicular, and the ones in the lower translation domain are oblique to sub-parallel, to the transport direction.

Fig. 11.--- Toe domain of the Gorgon Slide. **A)** Basal-shear surface variance map (top) and its interpretation (bottom). **B)** Internal body RMS amplitude map (time-slice at the orange horizon in D) (top) and its interpretation (bottom). **C)** Top surface dip map (top) and its interpretation (bottom). **D)** Seismic sections, uninterpreted (above) and interpreted (bottom), showing seismic facies across the toe domain. See text for discussion.

Fig. 12.--- Schematic diagram of Gorgon Slide depicting three stages of emplacement processes. **A)** A failure event occurred. **B)** The slide split into two flow cells, Cell A and B, due to a cluster of megaclasts derived from the headwall and/or slope strata that acted as a flow obstacle. **C)** Cell A ceased, and its frontal margin is expressed on the seabed, while Cell B flowed beyond the limit of the dataset. See text for discussion.

Fig. 13.--- A) Variance map extracted along the orange horizon in C-D, overlaid by time structure map of thrusted megaclasts (see the red horizon in D, left). The thrusted megaclasts define the frontal margin of Cell A and lateral margin of Cell B. **B)** Variance map extracted along the basal-shear surface (yellow) in C-D, overlaid by time structure map of the basal megaclasts (see the red horizon in D, right). **C)** Uninterpreted, and **D)** interpreted seismic section across the thrusted and basal megaclasts. These megaclasts have similar dimension and seismic facies, thus, likely to have a similar origin. Vertical exagerration of the seismic sections is 20.

844 Fig. 1

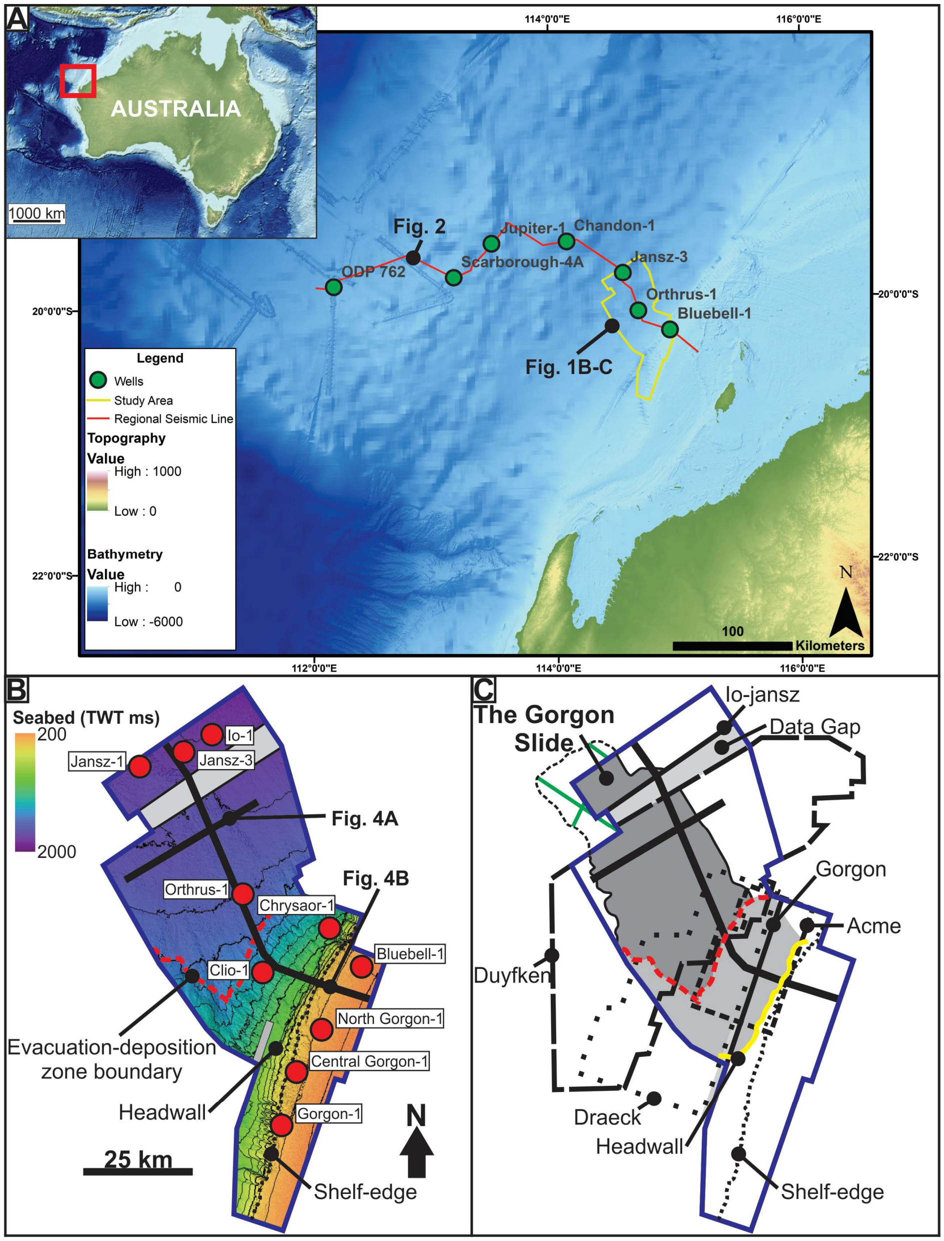
A
AUSTRALIA
1000 km
114°0'0"E
116°0'0"E
112°0'0"E
20°0'0"S
22°0'0"S
Fig. 2
ODP 762
Scarborough-4A
Jupiter-1
Chandon-1
Jansz-3
Orthrus-1
Bluebell-1
Fig. 1B-C
Legend
Wells
Study Area
Regional Seismic Line
Topography
Value
High : 1000
Low : 0
Bathymetry
Value
High : 0
Low : -6000
N
100
Kilometers
B
Seabed (TWT ms)
200
2000
Io-1
Jansz-1
Jansz-3
Fig. 4A
Fig. 4B
Orthrus-1
Chrysaor-1
Bluebell-1
Clio-1
North Gorgon-1
Central Gorgon-1
Gorgon-1
Evacuation-deposition zone boundary
Headwall
Shelf-edge
25 km
N
C
The Gorgon Slide
Io-jansz
Data Gap
Gorgon
Acme
Duyfken
Draeck
Headwall
Shelf-edge

845

Fig. 2

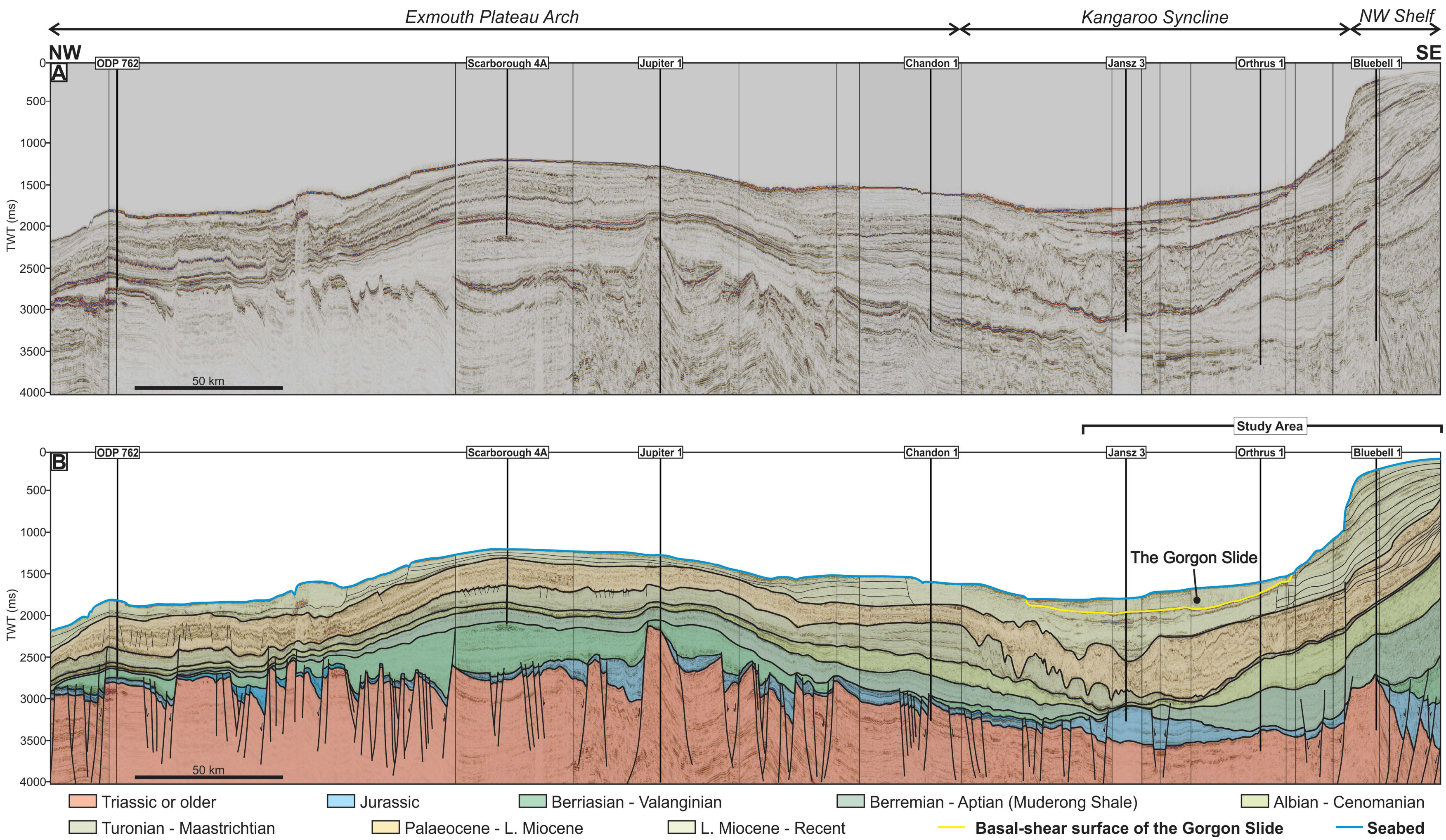
Exmouth Plateau Arch
Kangaroo Syncline
NW Shelf
NW
SE
A
B
ODP 762
Scarborough 4A
Jupiter 1
Chandon 1
Jansz 3
Orthrus 1
Bluebell 1
TWT (ms)
0
500
1000
1500
2000
2500
3000
3500
4000
50 km
Study Area
The Gorgon Slide
Triassic or older
Jurassic
Berriasian - Valanginian
Berremian - Aptian (Muderong Shale)
Albian - Cenomanian
Turonian - Maastrichtian
Palaeocene - L. Miocene
L. Miocene - Recent
Basal-shear surface of the Gorgon Slide
Seabed

Fig. 3

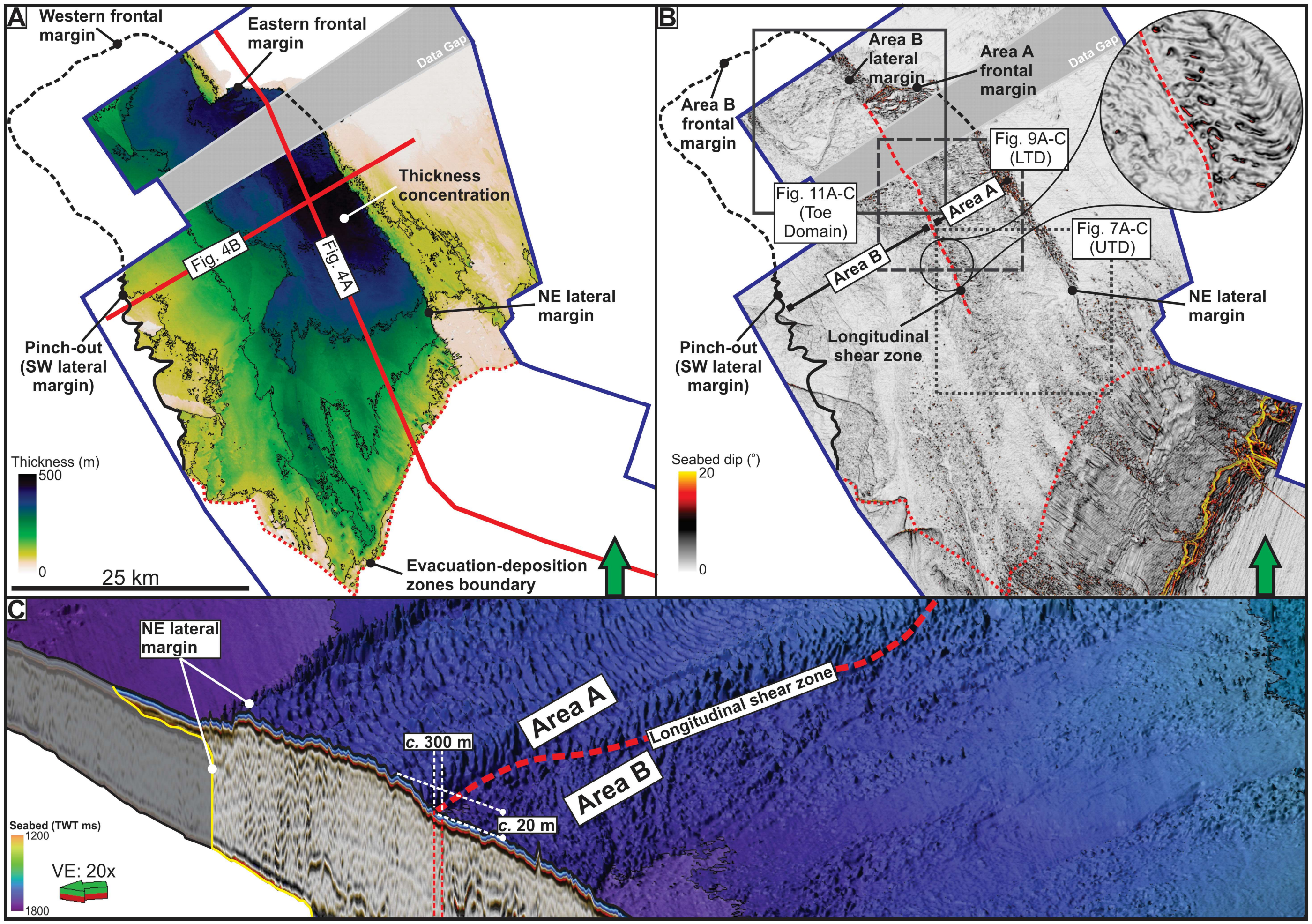
A
Western frontal margin
Eastern frontal margin
Data Gap
Thickness concentration
Fig. 4B
Fig. 4A
NE lateral margin
Pinch-out (SW lateral margin)
Thickness (m)
500
0
25 km
Evacuation-deposition zones boundary
B
Area B lateral margin
Area A frontal margin
Data Gap
Area B frontal margin
Fig. 9A-C (LTD)
Area A
Fig. 11A-C (Toe Domain)
Fig. 7A-C (UTD)
Area B
NE lateral margin
Pinch-out (SW lateral margin)
Longitudinal shear zone
Seabed dip (°)
20
0
C
NE lateral margin
Area A
Longitudinal shear zone
c. 300 m
Area B
c. 20 m
Seabed (TWT ms)
1200
1800
VE: 20x

Fig. 4

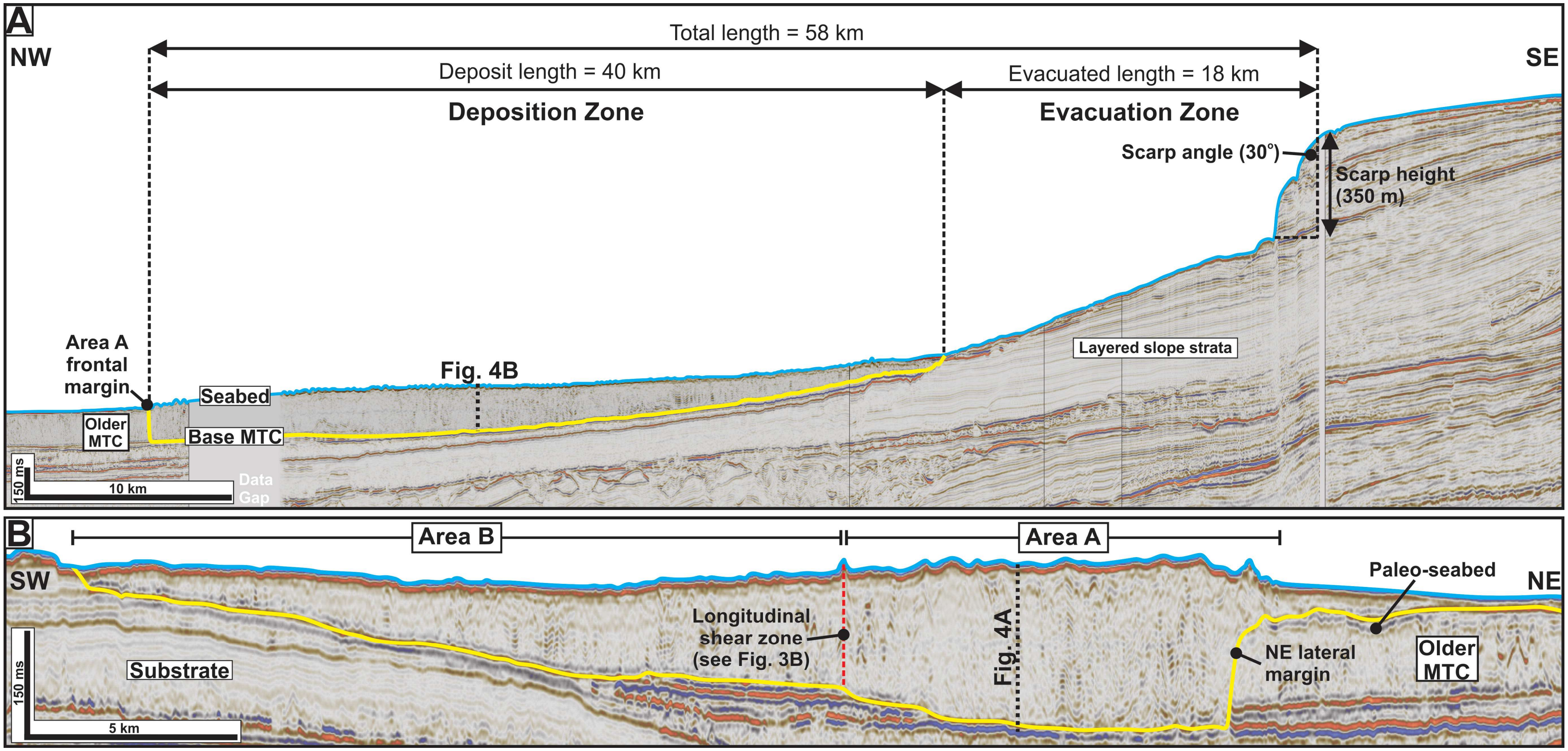
A
NW
SE
Total length = 58 km
Deposit length = 40 km
Evacuated length = 18 km
Deposition Zone
Evacuation Zone
Scarp angle (30°)
Scarp height
(350 m)
Layered slope strata
Area A
frontal
margin
Fig. 4B
Seabed
Older
MTC
Base MTC
Data
Gap
150 ms
10 km
B
Area B
Area A
SW
NE
Paleo-seabed
Longitudinal
shear zone
(see Fig. 3B)
Fig. 4A
NE lateral
margin
Older
MTC
Substrate
150 ms
5 km

Fig. 5

A Facies	Description	Interpretation
SF-1	Chaotic and transparent both in cross-section and map-view (Fig. 5B-C).	Debrites containing disaggregated materials (cf. Posamentier and Kolla 2003).
SF-2	Low-to-medium amplitude, discontinuous folded reflections that occasionally form sinuous lineations in map-view (Fig. 5B, D-E).	Debrites containing partially disaggregated materials (cf. Ortiz-Karpf et al. 2017).
SF-3	High amplitude, discontinuous folded reflections that are separated by imbricate thrusts (Fig. 5F-G).	Fold and thrust systems formed by compressional deformation within MTCs, flow direction is generally perpendicular to the strike of the thrusts (Bull et al. 2009).
SF-4	Isolated packages of coherent, sub-parallel reflections within a matrix composed of SF-1 or 2 (Fig. 5B-C, E). In most cases, the reflections are disrupted, e.g. faulted and folded.	Megaclasts transported within debritic matrix (cf. Bull et al. 2009; Jackson 2011; Hodgson et al. 2018).
SF-5	Medium-to-high amplitude, continuous, sub-parallel, downslope-dipping reflections beneath the shelf and within the evacuation zone (Fig. 4A).	Non-MTC deposits, i.e. carbonate progradation and layered slope deposits that were the source of, and eroded by, the Gorgon Slide (Hengesh et al. 2013; Nugraha et al. 2019b).

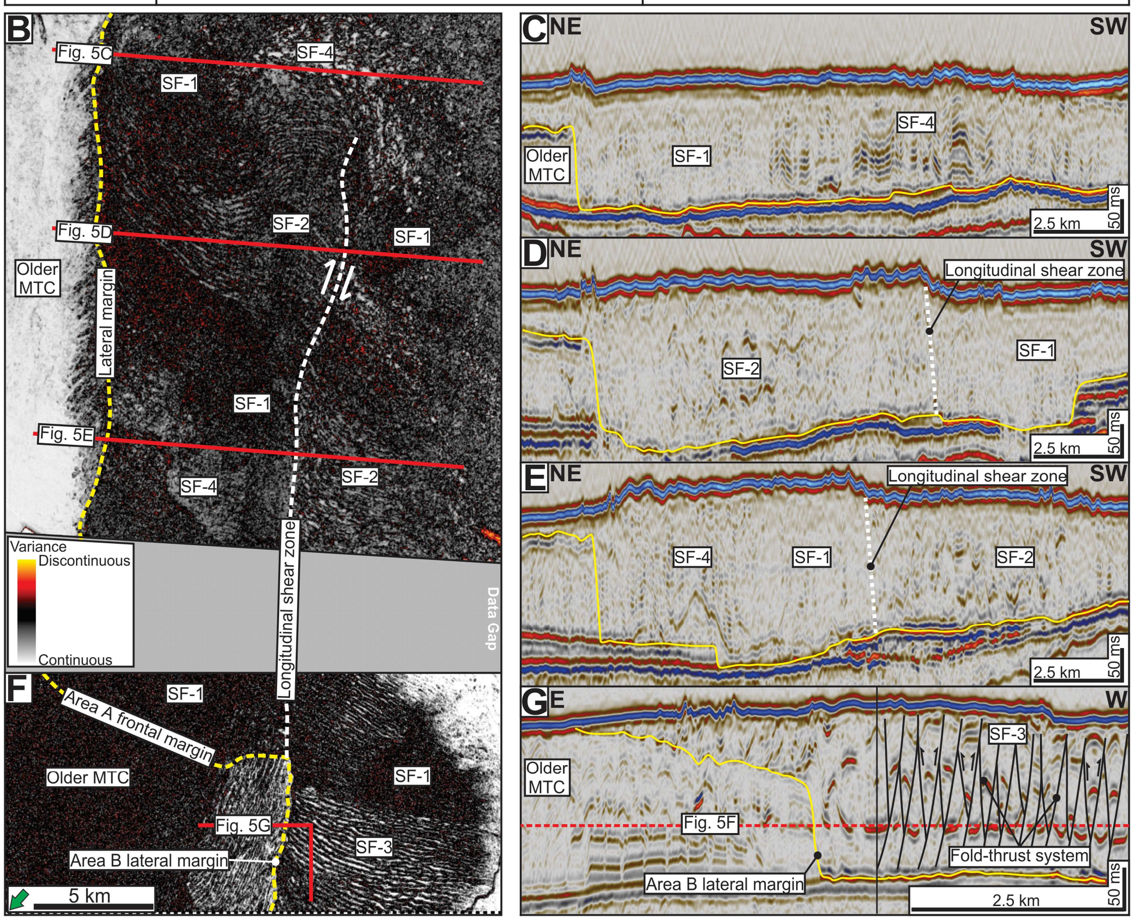

857 Fig. 6

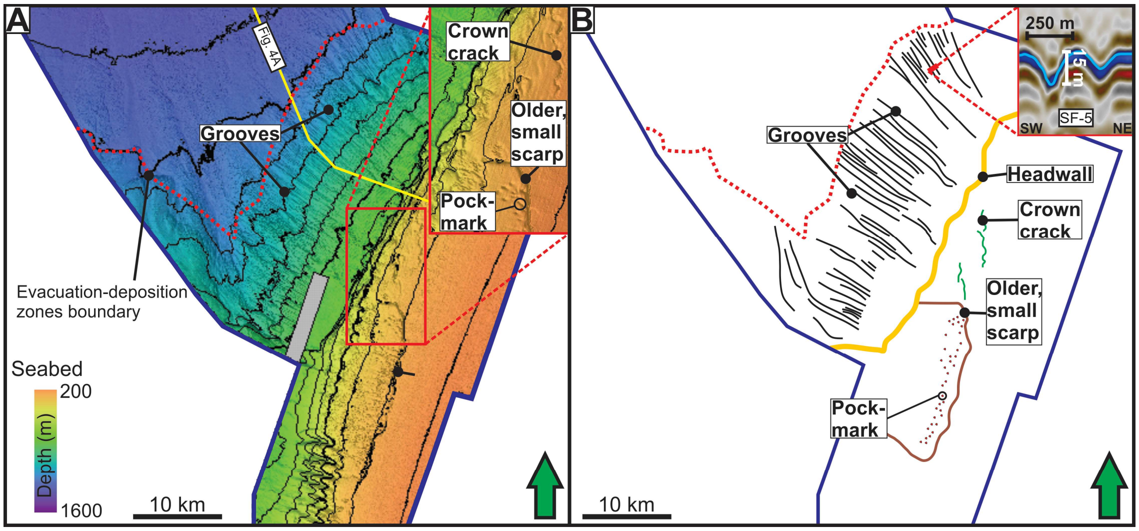

858

859

860 Fig. 7

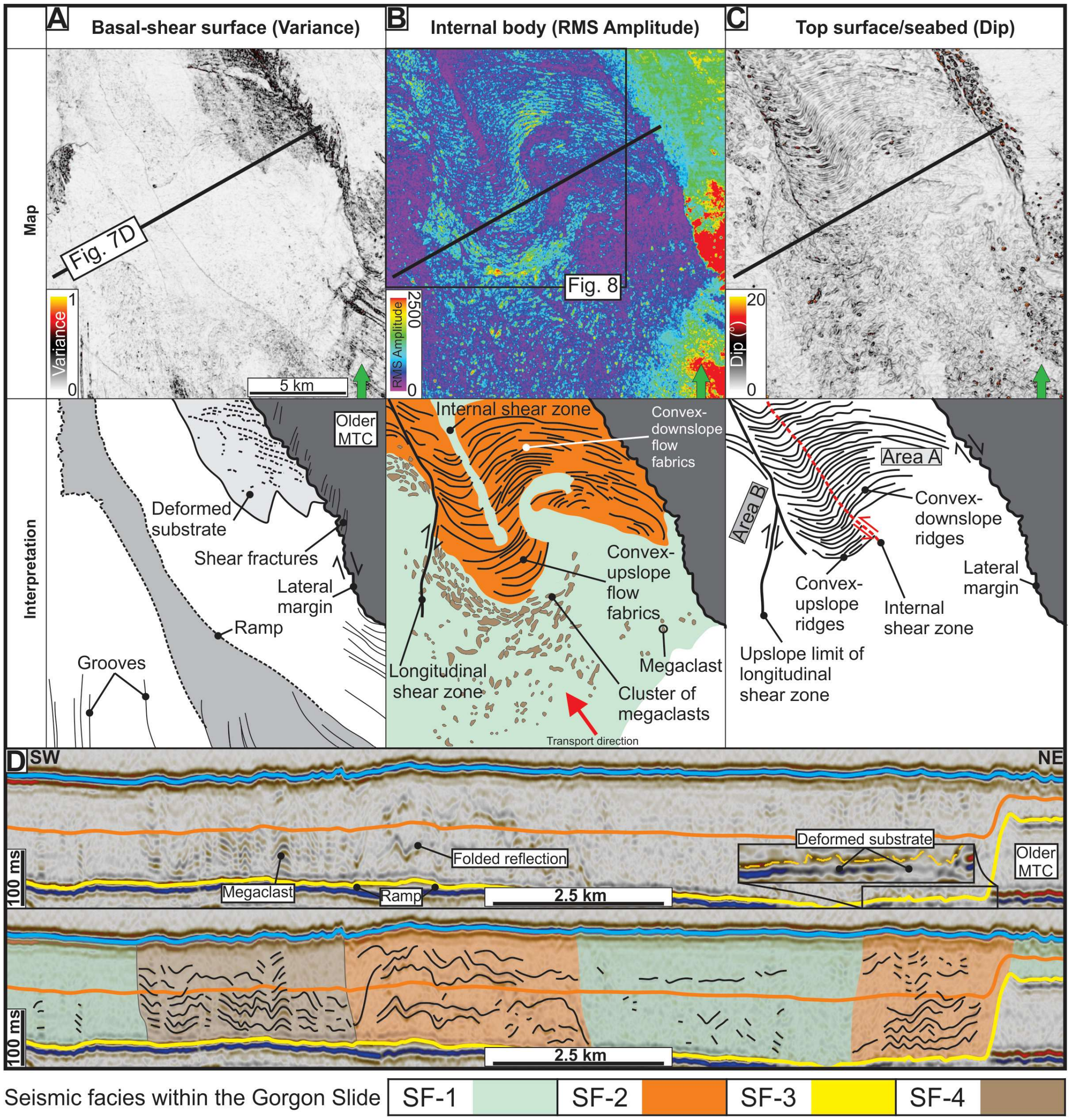

861

862

Fig. 8

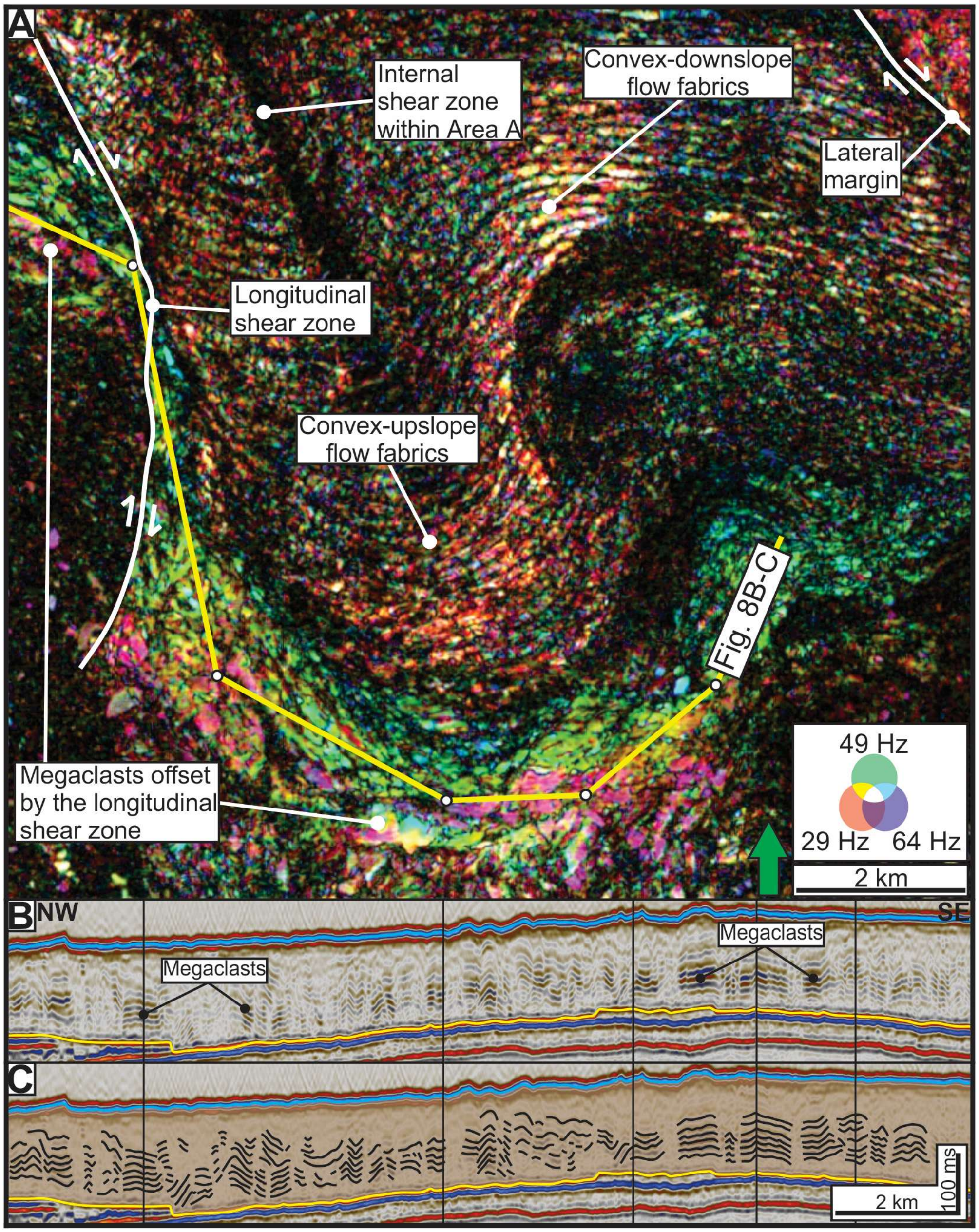
A
Internal
shear zone
within Area A
Convex-downslope
flow fabrics
Lateral
margin
Longitudinal
shear zone
Convex-upslope
flow fabrics
Fig. 8B-C
Megaclasts offset
by the longitudinal
shear zone
49 Hz
29 Hz
64 Hz
2 km
B
NW
SE
Megaclasts
Megaclasts
C
100 ms
2 km

Fig. 9

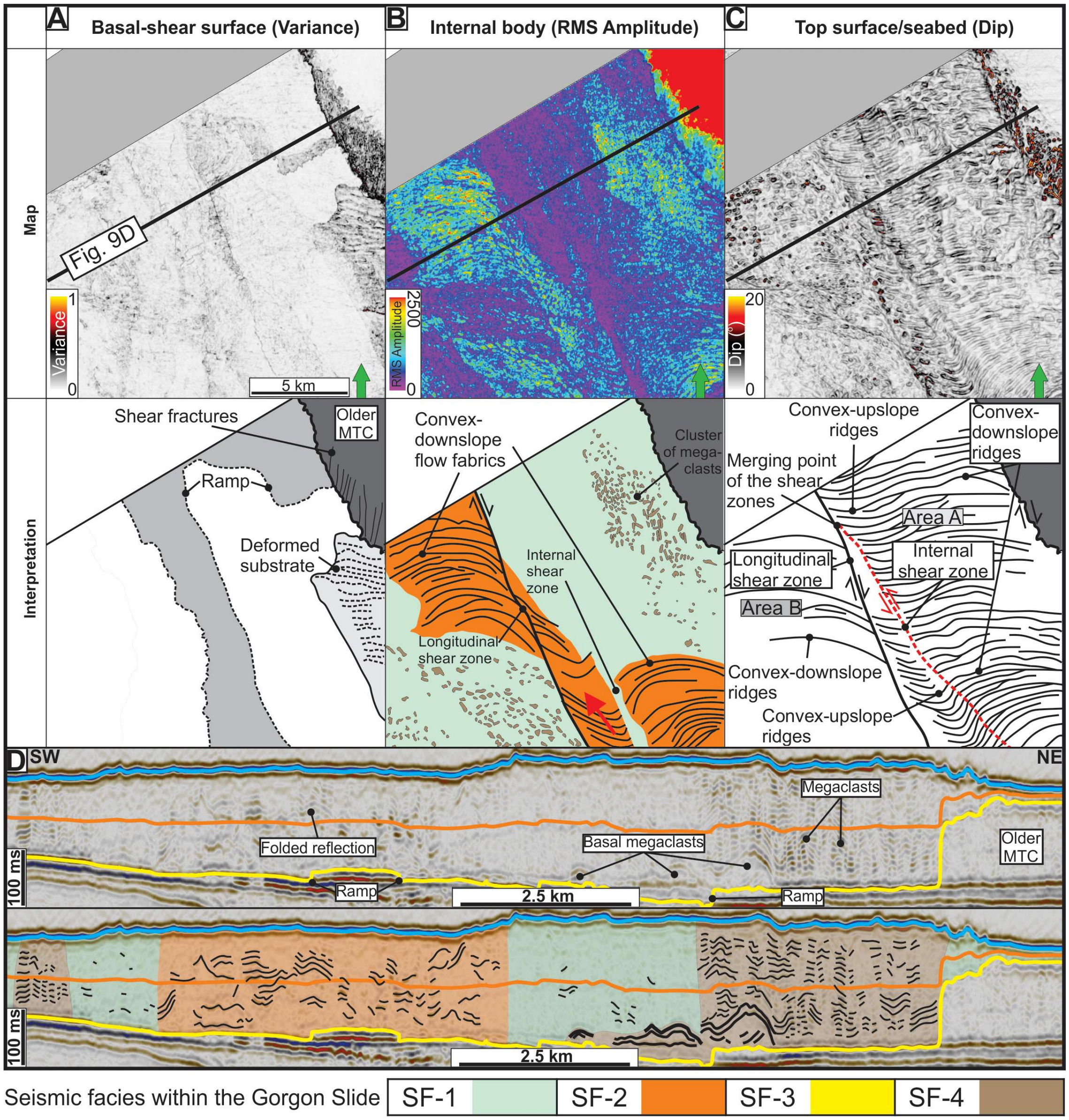
A
Basal-shear surface (Variance)
B
Internal body (RMS Amplitude)
C
Top surface/seabed (Dip)
Map
Interpretation
Fig. 9D
Variance
1
0
5 km
RMS Amplitude
2500
0
Dip (°)
20
0
Shear fractures
Older MTC
Ramp
Deformed substrate
Convex-downslope flow fabrics
Cluster of mega-clasts
Internal shear zone
Longitudinal shear zone
Convex-upslope ridges
Convex-downslope ridges
Merging point of the shear zones
Area A
Longitudinal shear zone
Internal shear zone
Area B
Convex-downslope ridges
Convex-upslope ridges
D
SW
NE
Megaclasts
Folded reflection
Basal megaclasts
Older MTC
100 ms
Ramp
2.5 km
Ramp
100 ms
2.5 km
Seismic facies within the Gorgon Slide
SF-1
SF-2
SF-3
SF-4

Fig. 10

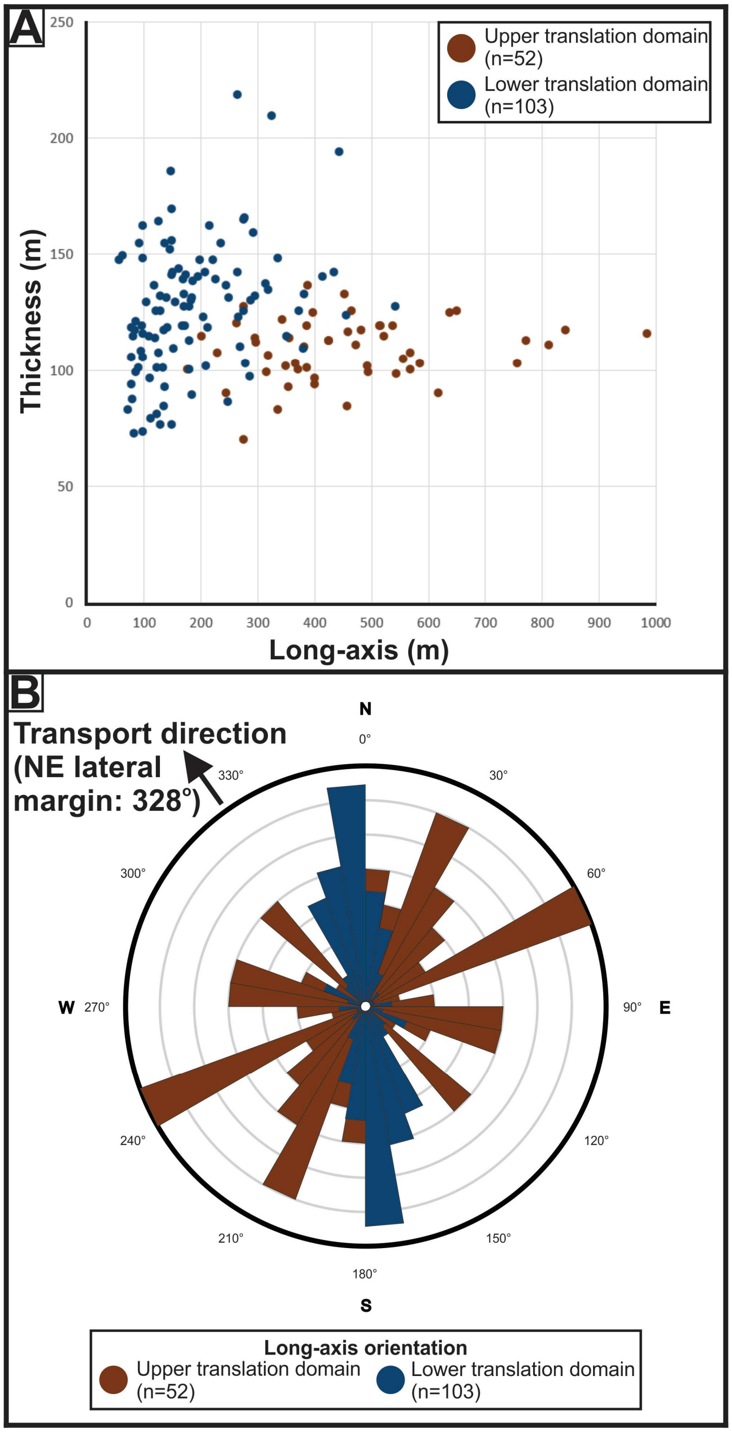
A
Upper translation domain (n=52)
Lower translation domain (n=103)
Thickness (m)
Long-axis (m)
0
50
100
150
200
250
0
100
200
300
400
500
600
700
800
900
1000
B
Transport direction (NE lateral margin: 328°)
N
0°
30°
60°
90°
E
120°
150°
180°
S
210°
240°
W 270°
300°
330°
Long-axis orientation
Upper translation domain (n=52)
Lower translation domain (n=103)

Fig. 11

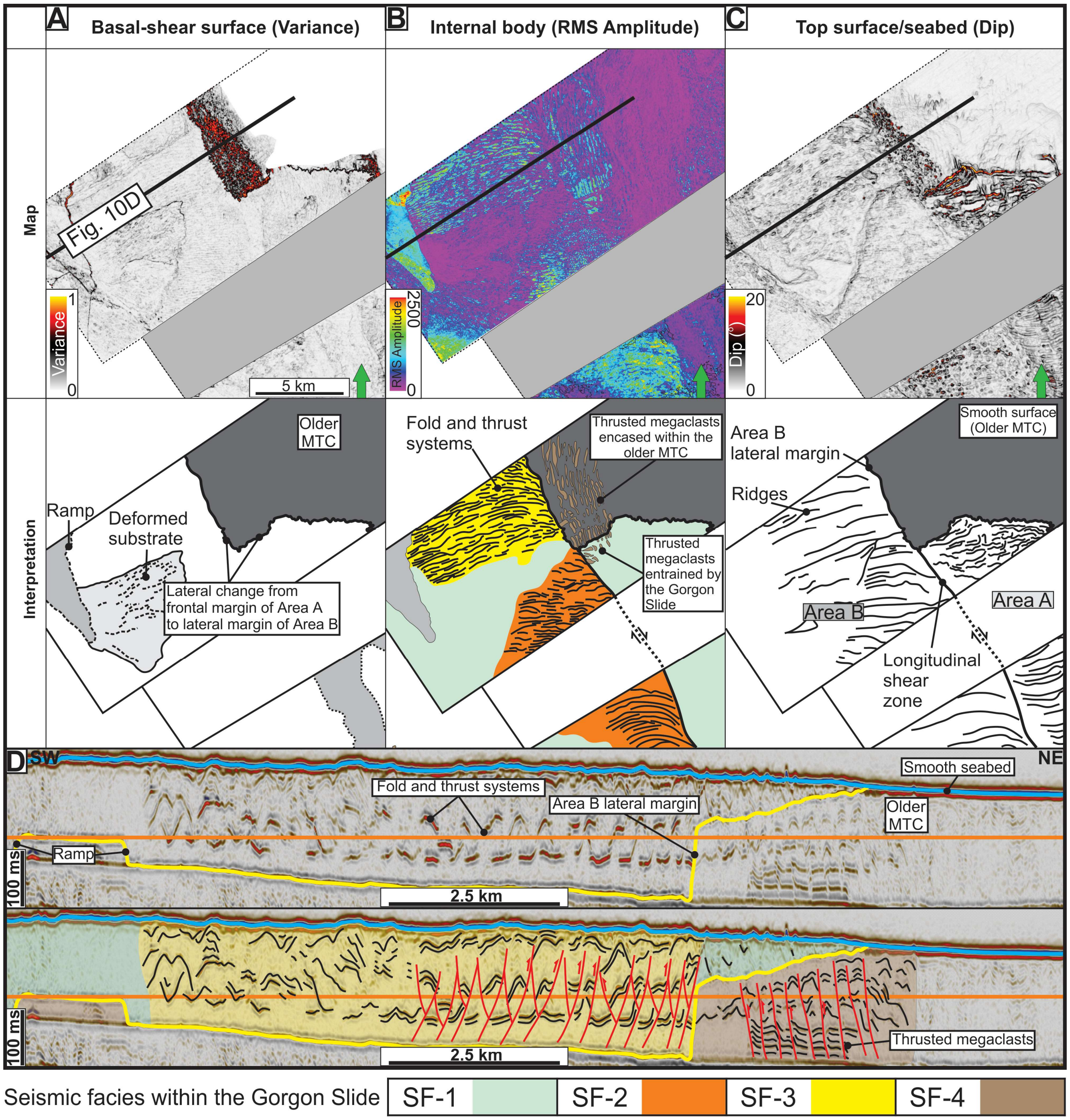
A
Basal-shear surface (Variance)
B
Internal body (RMS Amplitude)
C
Top surface/seabed (Dip)
Map
Interpretation
Fig. 10D
Variance
1
0
5 km
RMS Amplitude
2500
0
Dip (°)
20
0
Older MTC
Ramp
Deformed substrate
Lateral change from frontal margin of Area A to lateral margin of Area B
Fold and thrust systems
Thrusted megaclasts encased within the older MTC
Thrusted megaclasts entrained by the Gorgon Slide
Smooth surface (Older MTC)
Area B lateral margin
Ridges
Area B
Area A
Longitudinal shear zone
D
SW
NE
Smooth seabed
Fold and thrust systems
Area B lateral margin
Older MTC
Ramp
100 ms
2.5 km
Thrusted megaclasts
Seismic facies within the Gorgon Slide
SF-1
SF-2
SF-3
SF-4

Fig. 12

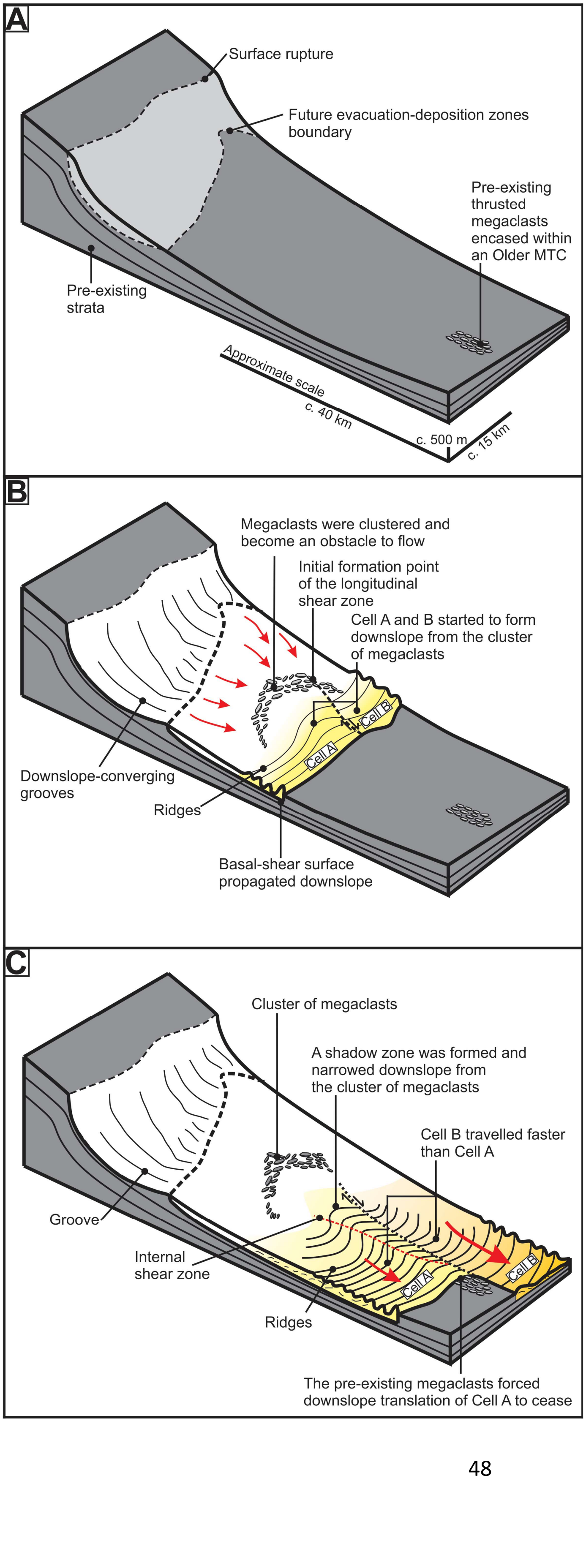
A
Surface rupture
Future evacuation-deposition zones boundary
Pre-existing thrusted megaclasts encased within an Older MTC
Pre-existing strata
Approximate scale
c. 40 km
c. 500 m
c. 15 km
B
Megaclasts were clustered and become an obstacle to flow
Initial formation point of the longitudinal shear zone
Cell A and B started to form downslope from the cluster of megaclasts
Cell A
Cell B
Downslope-converging grooves
Ridges
Basal-shear surface propagated downslope
C
Cluster of megaclasts
A shadow zone was formed and narrowed downslope from the cluster of megaclasts
Cell B travelled faster than Cell A
Groove
Internal shear zone
Ridges
Cell A
Cell B
The pre-existing megaclasts forced downslope translation of Cell A to cease

877 Fig. 13

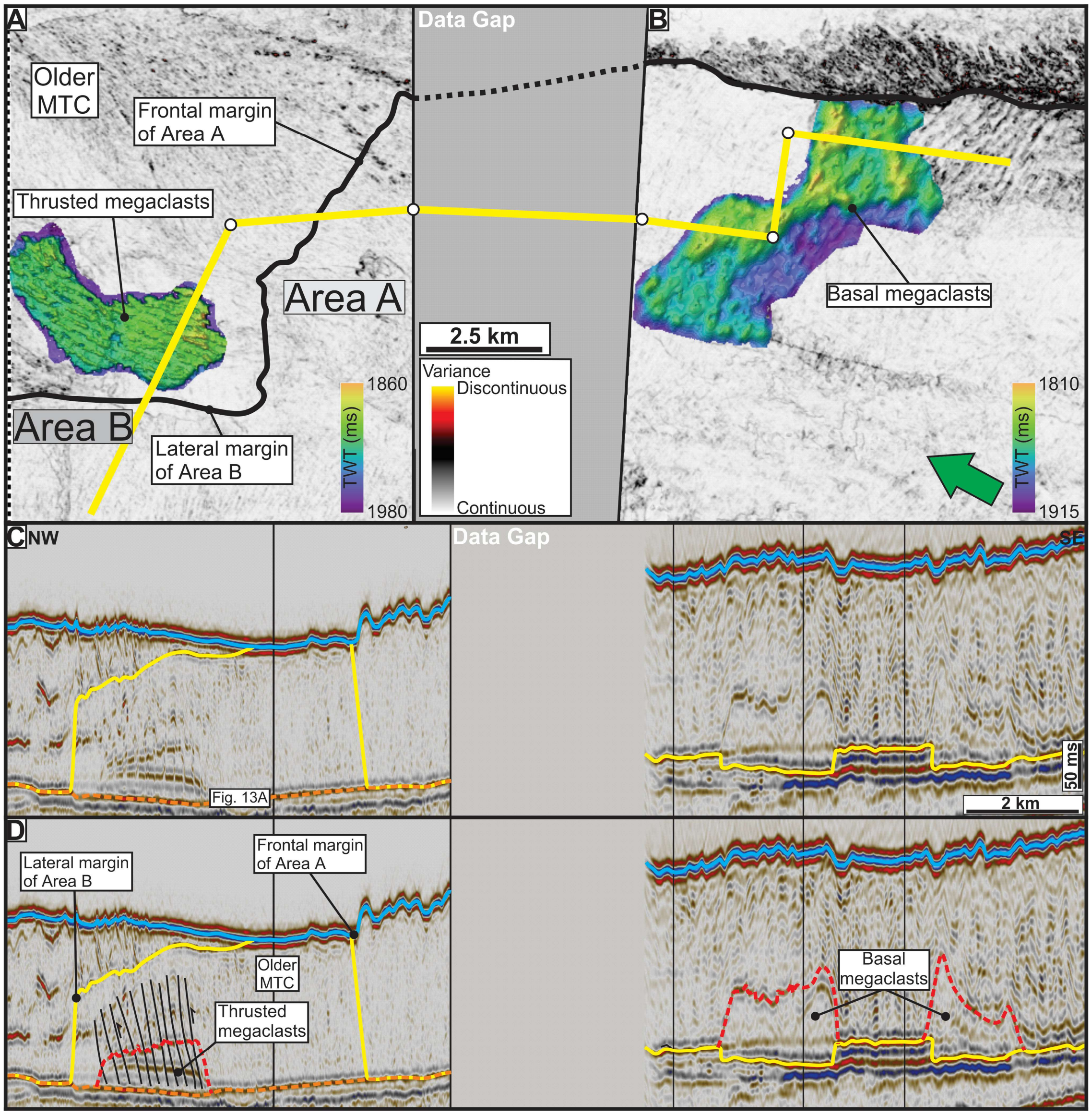

878